Experimental investigation of effective modulus of elasticity and shear modulus of brick masonry wall under lateral load

by

Taohida Parvin Akhi

A thesis submitted to the Faculty of Graduate Studies of
The University of Manitoba
in partial fulfilment of the requirements of the degree of

Master of Science

Department of Civil Engineering
Faculty of Engineering
University of Manitoba
Winnipeg, Manitoba

February 2012

Abstract

The primary objective of this research program was to investigate the effective modulus of elasticity and shear modulus of brick masonry walls under lateral load, and to to justify using the Jaeger and Mufti method to calculate the effective modulus of elasticity and shear modulus of brick masonry walls. The experimental program involved the testing of three unreinforced brick masonry walls under in-plane and vertical loads. Linear Variable Differential Transducers were used to record the horizontal and vertical displacements of the walls. The experimental results were used to evaluate the modulus of elasticity and the shear modulus of walls under flexure. The experimental results were compared to the finite element analysis results. It was found that the finite element analysis yields similar results to the experimental results. It was also found that the Jaeger and Mufti method to calculate effective modulus of elasticity and shear modulus of brick masonry walls is effective for design purposes.

Acknowledgments

I would like to acknowledge the support of several individuals without which completion of this thesis would not have been possible.

In the first place I would like to express my deepest gratitude to my supervisor Dr. Aftab A. Mufti, whose encouragement, guidance and support from the initial to the final level enabled me to develop an understanding of the subject. It has been an honour for me to be one of the members of his research group.

I owe my deepest gratitude to Dr. Leslie G. Jaeger for his advice, supervision, and crucial contribution, which made him a backbone of this research. I would like to show my gratitude to Dr. Baidar Bakht and Dr. Douglas Thomson for their comprehensive assistance in reviewing and editing this thesis, and their helpful suggestions on improving the final outcome.

Special thanks to Fariborz Hashemian and Dr. Amr El Ragaby who have made available their support in a number of ways.

The help of the technical staffs: Chad Klowak, Hughes Vogel, and Grant Whiteside is highly appreciated for their technical support and valuable assistance during fabrication,

construction and testing of the specimens. I am indebted to all the staffs of ISIS Canada Research Network and many of my colleagues to support me.

Finally, I would also like to convey my thanks to Public Works and Government Services Canada, and the ISIS Canada Research Network of Centres of Excellence for providing the financial supports. I am also thankful to Alpha Masonry©, Manitoba for the supply of technical supports.

Dedication

This thesis report is dedicated to my parents *Late M. A. Ahamed* and *Zaheda Khatoon* for their loving support throughout my years as a student.

Contents

Front Matter

List of Tables

List of Figures

List of Copyrighted Materials

Title of copyright items	Source	Page no. in this thesis report
Masonry Design for Engineers and Architects. By: M. Hatzinikolas, Y. Korany.	Canadian Masonry Publications, Edmonton, Alberta, Canada, pp. 200, 2005.	8, 63

List of Symbols

a	Width of masonry wall
b	Thickness of masonry wall
$[B]$	Strain matrix
$[D]$	Elasticity matrix
$(\frac{dp}{d\delta})$	Slope of active part of load-deflection curve up to cracking
E	Modulus of elasticity of masonry wall
e	Masonry strain
e_0	Masonry strain corresponding to the maximum stress
f	Masonry stress
f'_m	Compressive stress of masonry wall or masonry prism
G	Shear modulus of rigidity of masonry wall
h	Height of masonry wall
h_p	Height of masonry prism

I Moment of inertia for the gross section of masonry wall

$|J|$ Jacobian matrix

K Stiffness of element

P Applied horizontal load

r An arbitrary parameter

t Thickness of an element of finite element model

t_p Thickness of masonry prism

w_p Width of masonry prism

δ Horizontal deflection at top of the masonry wall

δ_1 Lateral deflection of the masonry wall of height h

δ_2 Lateral deflection of the masonry wall of height $2h$

List of Abbreviations and Acronyms

ASTM	American Society for Testing and Materials
CSA	Canadian Standard Association
DAQ	Data Acquisition System
FEA	Finite Element Analysis
FEM	Finite Element Model
LMT	Linear Motion Tandem Transducer
LVDT	Linear Variable Displacement Transducer
UMW	Unreinforced Masonry Wall

Chapter 1

Introduction

1.1 Overview

This thesis report describes the experimental investigation of the effective modulus of elasticity (*E*) and shear modulus (*G*) of brick masonry walls under lateral loads. There are six chapters in this report. Chapter 1 discusses the background, objective and scope of this research project. In Chapter 2, a brief literature review is presented. The details of specimens, experimental setup, and instrumentation procedure are explained in Chapter 3. Chapter 4 presents the experimental results. In Chapter 5, the analysis of experimental data is presented. The research findings, conclusion and recommendations for future research are presented in Chapter 6.

1.2 Background

The performance of a masonry wall in bending and shear is critical due to its low tensile strength. Masonry is a non-homogeneous and anisotropic material. As a result, its behaviour in shear and under compressive loads is different from that of homogeneous and isotropic materials. Under lateral loads the load bearing masonry wall acts as a shear wall. The behaviour of a masonry wall under lateral loads depends on various factors, such as: the magnitude of vertical load, ratio of wall height to length, properties of brick and mortar. Many experimental studies have been undertaken to evaluate different factors related to the lateral resistance of masonry walls, and to predict the behaviour of masonry under in-plane forces. This experimental study was conducted to study the performance of masonry walls under in-plane forces and to estimate their effective modulus of elasticity and shear modulus under lateral loads.

1.3 Research objectives

The primary objective of the research study was to estimate effective modulus of elasticity (E) and shear modulus (G) of brick masonry walls in flexure, when displacements are so small that cracking of mortar does not occur. The experimental results were compared to the E and G values of masonry walls obtained using the procedure specified in the CSA standard (*CSA 2004*). In addition, the experimental results were also compared to the E and G values of masonry walls obtained using the method proposed by Jaeger and Mufti (Jaeger and Mufti method) (*Jaeger et al. 2010*),

and the finite element analysis results. Based on the primary objectives, several goals were set for the research project as summarized below:

- Determine the effective modulus of elasticity (*E*) and shear modulus (*G*) of brick masonry walls in flexure by experimental investigation.
- Study the mode of failures of the masonry walls in flexure.
- Compare the experimental results with theoretical results obtained using the CSA standard, the Jaeger and Mufti method, and the finite element analysis.
- Validate the Jaeger and Mufti method by laboratory tests and finite element analysis of the models.
- Justify the possibility of using the test procedure to determine the modulus of elasticity (*E*) and shear modulus (*G*) of brick masonry walls in flexure.

1.4 Scope of work

The scope of the work was planned to achieve the objectives of the research project that encompassed different aspects of structural engineering. The variables of the research project were the brick and mortar strength, wall height and width. The results obtained from the laboratory tests were the first cracking load, wall deflection (horizontal, vertical) and crack pattern. The work included:

- Design and construction of three masonry walls.

- Design and construction of load beam and load frame.
- Design and installation of instruments to record the experimental results.
- Design of test procedure.
- Conducting the laboratory tests.
- Analysis of test results.
- Comparing of the experimental results with theoretical results obtained using the CSA standard, the Jaeger and Mufti method, and finite element analysis.

The subsequent chapters will describe about the above mentioned working steps in detail.

Chapter 2

Literature Review

2.1 General

One of the oldest construction materials used to build structures around the world is masonry. It has been used as a structural element for thousands of years. Not only have most of the historical buildings been built of unreinforced clay brick masonry but also many nuclear power plants of the 20th century. A large number of existing masonry buildings in Canada have been constructed in the last 200 years. Over the years, the integrity of these old masonry buildings has been declining. One of the main reasons for this deterioration is related to the fact that these structures have not been designed to resist lateral earthquake forces but mainly to resist vertical loading. Since masonry structures are weaker in tension than they are in compression, they are more vulnerable to failure under lateral than vertical loads. The failure of masonry walls also depends on the bond between the mortar and masonry units. The effective design, repair and strengthening of masonry buildings therefore require sound knowledge of the behaviour

of masonry materials and structures along with the methods involved in their construction.

The behaviour of masonry walls in seismic areas is influenced by several factors. One of the main factors is the performance under in-plane lateral load, which is further related to various parameters including the properties of masonry components and their performance under lateral load.

2.2 Common types of failure of masonry walls under lateral load

An Unreinforced Masonry Wall (UMW) is vulnerable to earthquake. During an earthquake, the wall experiences lateral loads along with the vertical gravity loads. An UMW behaves like a brittle material. As a result brittle failure occurs in UMW when the state of stress in the wall exceeds the strength of masonry. This failure leads to the collapse of the wall. Masonry walls subjected to in-plane loads exhibit three types of failure as illustrated in Figure 1. The blue lines in the figures indicate cracks.

The most common type of failure of masonry walls is shear failure which might occur in walls subjected to significant vertical and horizontal loads. Usually the aspect ratio for such a wall is about 1:1. In the case of higher vertical loads, this type of failure might occur in masonry walls having a higher aspect ratio such as 2:1.

If the masonry wall with poor shear strength is loaded predominantly by horizontal forces, the wall might exhibit sliding shear. Usually the aspect ratio for such a wall is about 1:1 or less (1:1.5).

Bending failure is common in the masonry walls with higher shear resistance. For walls of higher aspect ratio (2:1), small vertical load might initiate this type of failure. During this type of failure the whole masonry panel might rock like a rigid body.

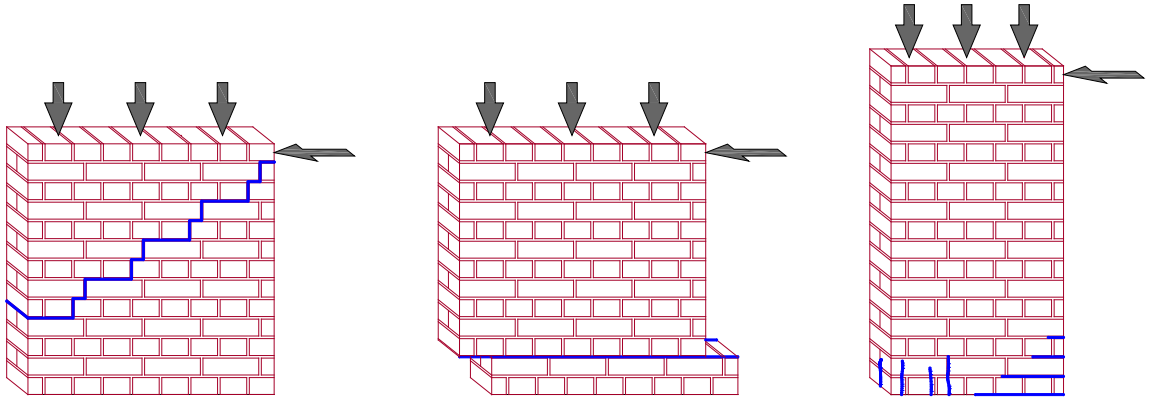

(a) Shear **(b) Sliding shear** **(c) Bending**

Figure 1: Different types of failure of masonry walls under lateral loads

2.3 Different methods to determine effective modulus of elasticity and shear modulus of brick masonry wall under lateral loads

2.3.1 Canadian Standard Association (CSA) specifications

According to article 6.5.2 of Canadian Standard Association *(CSA 2004)*, the modulus of elasticity (*E*) of masonry wall is calculated by the following equation:

$$E = 850f'_m \quad (1)$$

Where, f'_m is the compressive strength of masonry prism determined by the ASTM C109/C109M -07 (*ASTM 2007-a*) standard specifications, and the value of *E* should not greater than 20,000 MPa .

Conventionally (*Hatzinikolas et al. 2005*) the shear modulus or modulus of rigidity of masonry wall (*G*) is considered as 40% of the modulus of elasticity of masonry wall (*E*), i.e.:

$$G = 0.4E \quad (2)$$

2.3.2 Jaeger and Mufti method

According to Dr. Leslie G. Jaeger and Dr. Aftab A. Mufti *(Jaeger et al., 2010)*, unreinforced masonry walls are more vulnerable to shear than to flexure. According to

the researchers, the modulus of elasticity and shear modulus of unreinforced brick masonry walls subjected to lateral loads will be lower than the traditional values, which are estimated for masonry walls subjected to compressive loads. Moreover, estimating the uncracked value of the modulus of elasticity under lateral load is an important parameter for the resistance of masonry walls to shear effects in earthquake-prone areas. When unreinforced masonry walls are subjected to earthquake loads, cracks propagate through the mortar joints and sometimes through the bricks. These cracks reduce the effective modulus of elasticity and shear modulus of elasticity of masonry walls.

Considering the above mentioned situation, Dr. Jaeger and Dr. Mufti proposed a new method to calculate the effective modulus of elasticity and shear modulus of brick masonry wall under in-plane lateral loads. This method is referred to as the Jaeger and Mufti method in this research report. According to them, if a cantilever masonry wall having dimension of a (length) × b (width) × h (height) is subjected to an in-plane horizontal load of magnitude P at the top as can be seen in Figure 2, the horizontal deflection (δ) at top of the masonry wall is given by the following equation:

$$\delta = \frac{Ph^3}{3EI} + \frac{Ph}{Gab}$$

$$\Rightarrow \delta = \frac{Ph^3}{3E \times \frac{ba^3}{12}} + \frac{Ph}{Gab}$$

$$\Rightarrow \delta = \frac{Ph}{ab}\left\{\frac{4}{E}\left(\frac{h}{a}\right)^2 + \frac{1}{G}\right\}$$

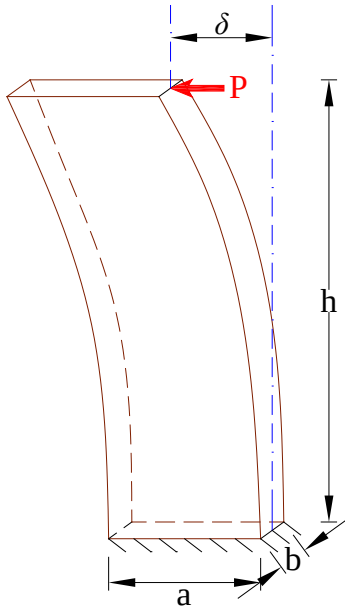

Figure 2: Deflection of masonry wall under lateral load

Here E is the modulus of elasticity, G is the shear modulus, and I is the moment of inertia for the gross section of masonry wall. Taking the derivative of horizontal deflection (δ) with respect to horizontal load (P) yields the slope of the horizontal load versus horizontal deflection graph:

$$\Rightarrow Slope = \frac{d\delta}{dP} = \frac{h}{ab}\left\{\frac{4}{E}\left(\frac{h}{a}\right)^2 + \frac{1}{G}\right\}$$

Replacing $E = r \times G$, where r is an arbitrary parameter and rearranging the above equation:

$$\Rightarrow G = \left(\frac{h}{ab}\right)\left(\frac{dP}{d\delta}\right)\left\{1 + \frac{4}{r}\left(\frac{h}{a}\right)^2\right\} \quad (3)$$

Where, $E = r \times G$ (4)

The Jaeger and Mufti method is to be validated following laboratory testing and finite element analysis of the models. The validation system is demonstrated in the flowchart presented in Figure 3. In order to validate the model using laboratory test, the monitoring system is to be tuned followed by monitoring the structure and evaluating the structural response. The validation through finite element analysis of the model is done by the modification of the finite element models followed by linear elastic analysis. The two validation systems are to be repeated until the accurate evaluation is achieved.

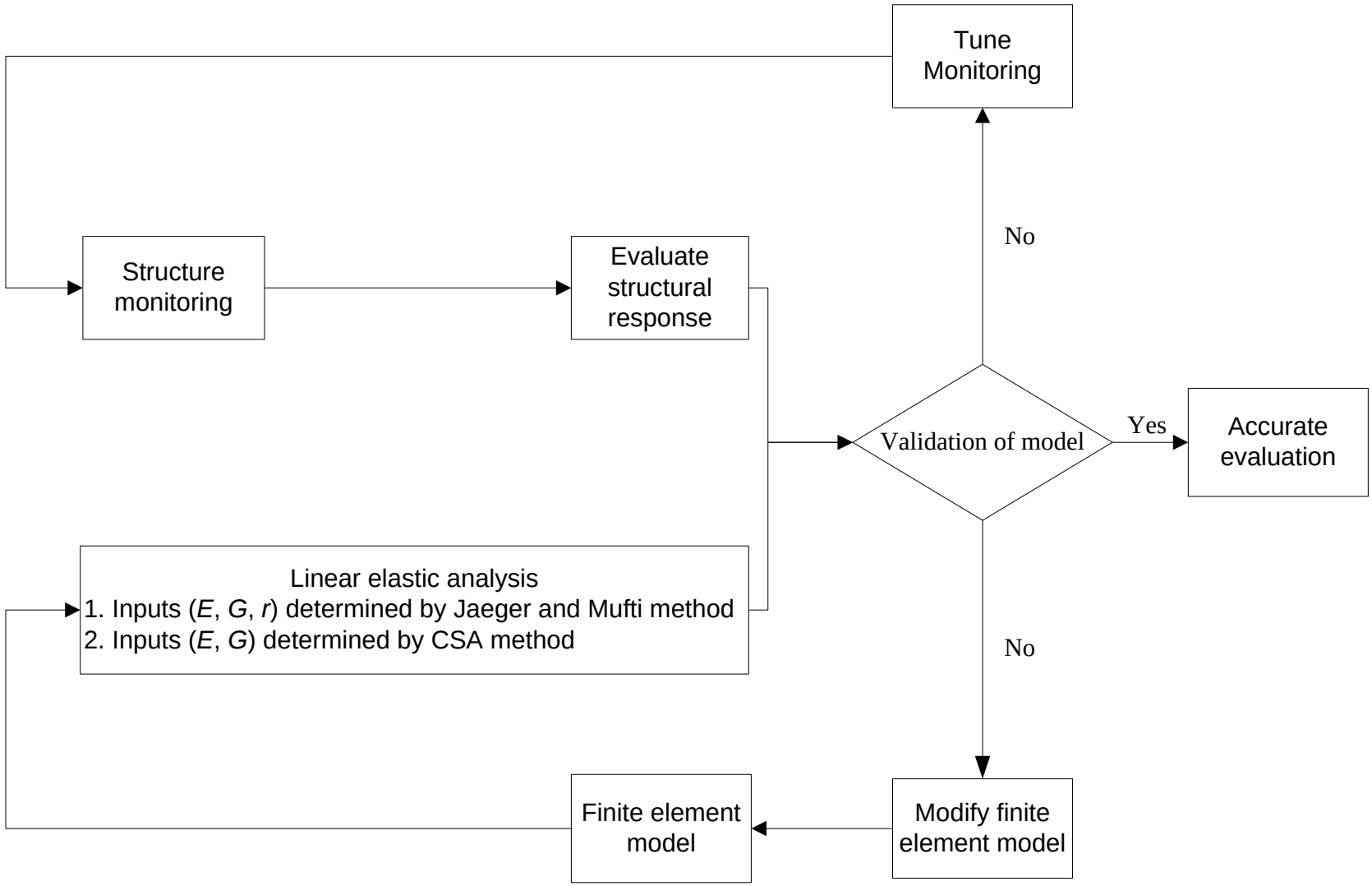

Figure 3: System identification using modelling and testing

2.3.3 Finite element analysis

A masonry wall is a composite material consisting of brick and mortar. Brick is the building unit and mortar is the jointing material. The mechanical property of the brick units and mortar influence the basic mechanical properties of the masonry wall. The finite element analysis of a masonry wall is complex due to the non-homogeneity of the constituents. One approach to solve the problem is to replace the constituents with a material having equivalent material properties, assuming it to be a homogenized material. A computer program *(Akhi et. al. 2011)* developed by Dr. Aftab A. Mufti using FORTRAN computer language was used to conduct the numerical analysis. The procedure used to conduct the numerical analysis of the masonry walls of this research program is described below.

The finite element method:

At first, the structure is divided into an assembly of isoparametric finite elements that are connected at the nodes. The minimum potential energy theorem is used to determine the stiffness characteristics of each element. The element geometry and natural coordinates can be seen in Figure 4.

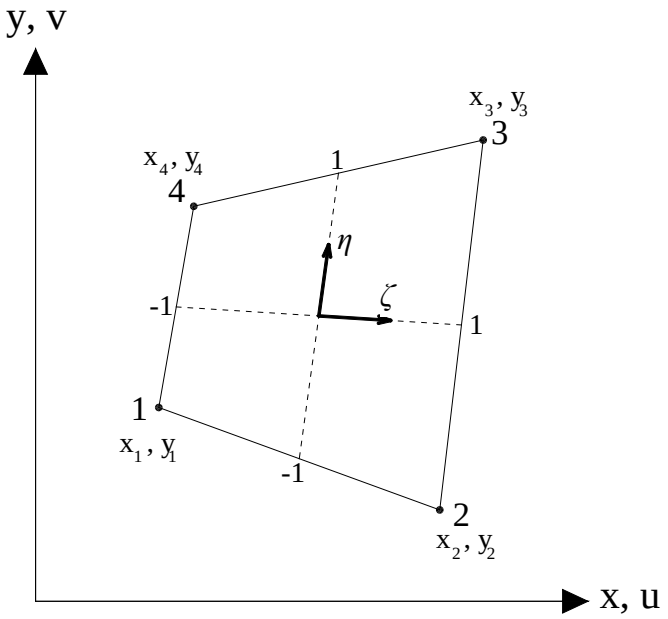

Figure 4: Natural coordinate system for isoparametric element

The following equations represent the plane stress case for the finite element analysis:

$$\begin{Bmatrix} x \\ y \end{Bmatrix} = \begin{bmatrix} N_1 & 0 & N_2 & 0 & N_3 & 0 & N_4 & 0 \\ 0 & N_1 & 0 & N_2 & 0 & N_3 & 0 & N_4 \end{bmatrix} \begin{Bmatrix} x_1 \\ y_1 \\ x_2 \\ y_2 \\ x_3 \\ y_3 \\ x_4 \\ y_4 \end{Bmatrix}$$

$$N_1 = \frac{(1-\zeta)(1-\eta)}{4} \qquad N_2 = \frac{(1+\zeta)(1-\eta)}{4}$$

$$N_3 = \frac{(1+\zeta)(1+\eta)}{4} \qquad N_4 = \frac{(1-\zeta)(1+\eta)}{4}$$

$$\underline{f} = \underline{N\delta}$$

$$f = \begin{Bmatrix} u \\ v \end{Bmatrix} = \begin{bmatrix} N_1 & 0 & N_2 & 0 & N_3 & 0 & N_4 & 0 \\ 0 & N_1 & 0 & N_2 & 0 & N_3 & 0 & N_4 \end{bmatrix} \begin{Bmatrix} u_1 \\ v_1 \\ u_2 \\ v_2 \\ u_3 \\ v_3 \\ u_4 \\ v_4 \end{Bmatrix}$$

$$\underline{\varepsilon} = \begin{Bmatrix} \dfrac{\partial u}{\partial x} \\ \dfrac{\partial v}{\partial y} \\ \dfrac{\partial u}{\partial y} + \dfrac{\partial v}{\partial x} \end{Bmatrix} = \underline{B}\ \underline{\delta_e}$$

$$\underline{P_e} = \underline{K_e}\ \underline{\delta_e}$$

$$K = t \int_{-1}^{1} \int_{-1}^{1} [B]^T\ [D]\ [B]\ |J|\ \partial\xi\ \partial\eta \qquad (5)$$

Where, K = stiffness of element

t = thickness of an element

$|J|$ = Jacobian matrix

[D] = elasticity matrix

[B] = strain matrix

The global stiffness matrix is obtained by adding the stiffness matrices from individual elements. The stresses and strains at the centroid of elements are determined from the displacements derived by solving the equilibrium equations.

Masonry elements:

The masonry elements are assumed to behave linearly in tension. The response in compression is represented using Saenz's non-linear stress-strain relationship. It is worth noting that the biaxial plane stress problem of masonry in compression and tension is generally examined using separate uniaxial stress-strain relationships. The nature and magnitude of the stresses acting on the element influence the general behaviour of masonry under combined stresses (strength, deformation, etc.). The expression shown below defines Saenz's equation for the stress-strain curve in compression.

$$f = \frac{E\,e}{1 + (R + R_E - 2)\frac{e}{e_0} - (2R - 1)\left(\frac{e}{e_0}\right)^2 + R(\frac{e}{e_0})^3} \tag{6}$$

where $R = \frac{R_E(R_f - 1)}{(R_e - 1)^2} - \frac{1}{R_e}$

$$R_E = \frac{E}{E_o}$$

$$R_f = \frac{f_0}{f_f}$$

$$R_e = \frac{e_f}{e_0}$$

f = masonry stress

f_f = maximum masonry stress at failure

e = masonry strain

e_f = maximum masonry strain at failure

e_0 = masonry strain corresponding to the maximum stress f_0

E = initial tangent modulus

$E_o = \frac{2f_0}{e_0}$ (assumed to be equal for tension and compression)

The tangent modulus of elasticity for the masonry elements at any stress is given by the following equation.

$$E_t = \frac{df}{de} = \frac{E\left[1 + (2R-1)\left(\frac{e}{e_0}\right)^2 - 2R\left(\frac{e}{e_0}\right)^3\right]}{\left[1 + (R+R_E-2)\left(\frac{e}{e_0}\right) - (2R-1)\left(\frac{e}{e_0}\right)^2 + R\left(\frac{e}{e_0}\right)^3\right]^2} \quad (7)$$

Analysis – incremental loading:

The investigation program uses an incremental loading procedure. The loads are increased from zero to failure in small increments.

First load increment:

The initial modulus of elasticity (E) is to be used to calculate the stiffness of all masonry elements. The strain and stresses calculated at the centroid of the masonry elements are

calculated by solving equilibrium equations for displacements. The crack initiation is checked by comparing the principal tensile stress at the centroid of each masonry element with the modulus of rupture of masonry.

Second and subsequent load increment:

The value of *E* obtained for the strain level, computed in the previous step for each element, is used to modify the stiffness of the masonry elements. The global stiffness matrix is formed by adding the modified stiffness from each element. This global stiffness matrix is then used to evaluate the displacements. The strains and stiffness at the centroid of the masonry elements are evaluated again and the check for crack initiation is repeated.

Masonry cracking:

A masonry element is considered to be cracked when the principal tensile stress at its centroid equals or exceeds the modulus of rupture. After the initiation of cracking in an element, the program modifies the thickness of the cracked element to zero. Thus, the contribution of the cracked element in the global stiffness matrix is eliminated. The equivalent forces at the nodes of the cracked element are applied to the surrounding masonry element to redistribute the forces present in the cracked masonry element.

Chapter 3

Experimental Program

3.1 Detail of specimens

In total, three unreinforced brick masonry walls were constructed and tested for this research program. The designation and dimensions of the masonry walls are presented in Table 1. The thickness of the walls was determined using the specifications of CSA S304.1-04 *(CSA 2004)*.

Table 1: Designation and dimensions of masonry walls

Specimen designation	Height, *h* (mm)	Width, *a* (mm)	Thickness, *b* (mm)
Wall-1	1000	1000	210
Wall-2	1500	1000	210
Wall-3	2000	1000	210

Detail of the masonry wall specimens are demonstrated in Figure 5, Figure 6 and Figure 7. One of the walls can be seen in Figure 8.

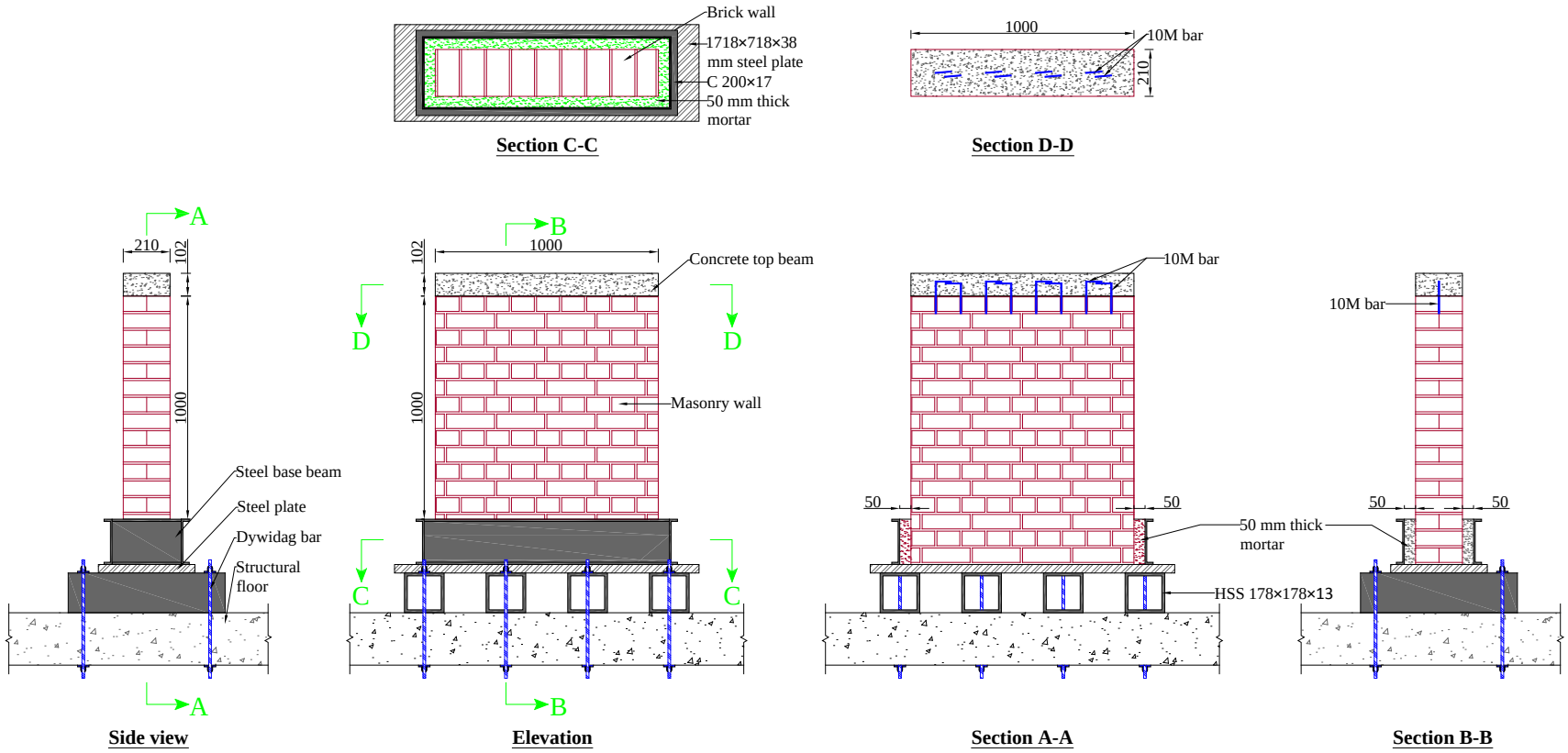

Figure 5: Details of Wall-1

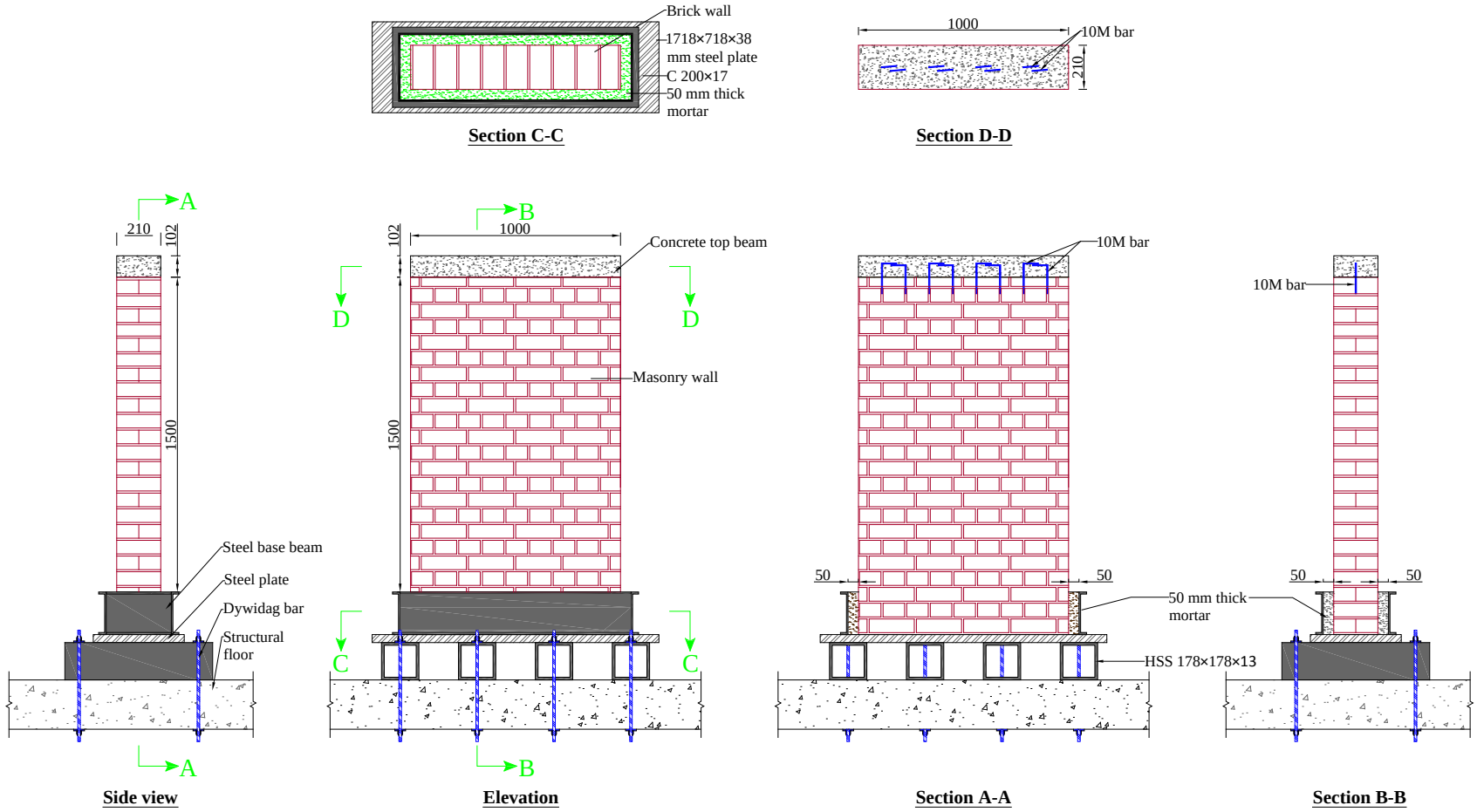

Figure 6: Details of Wall-2

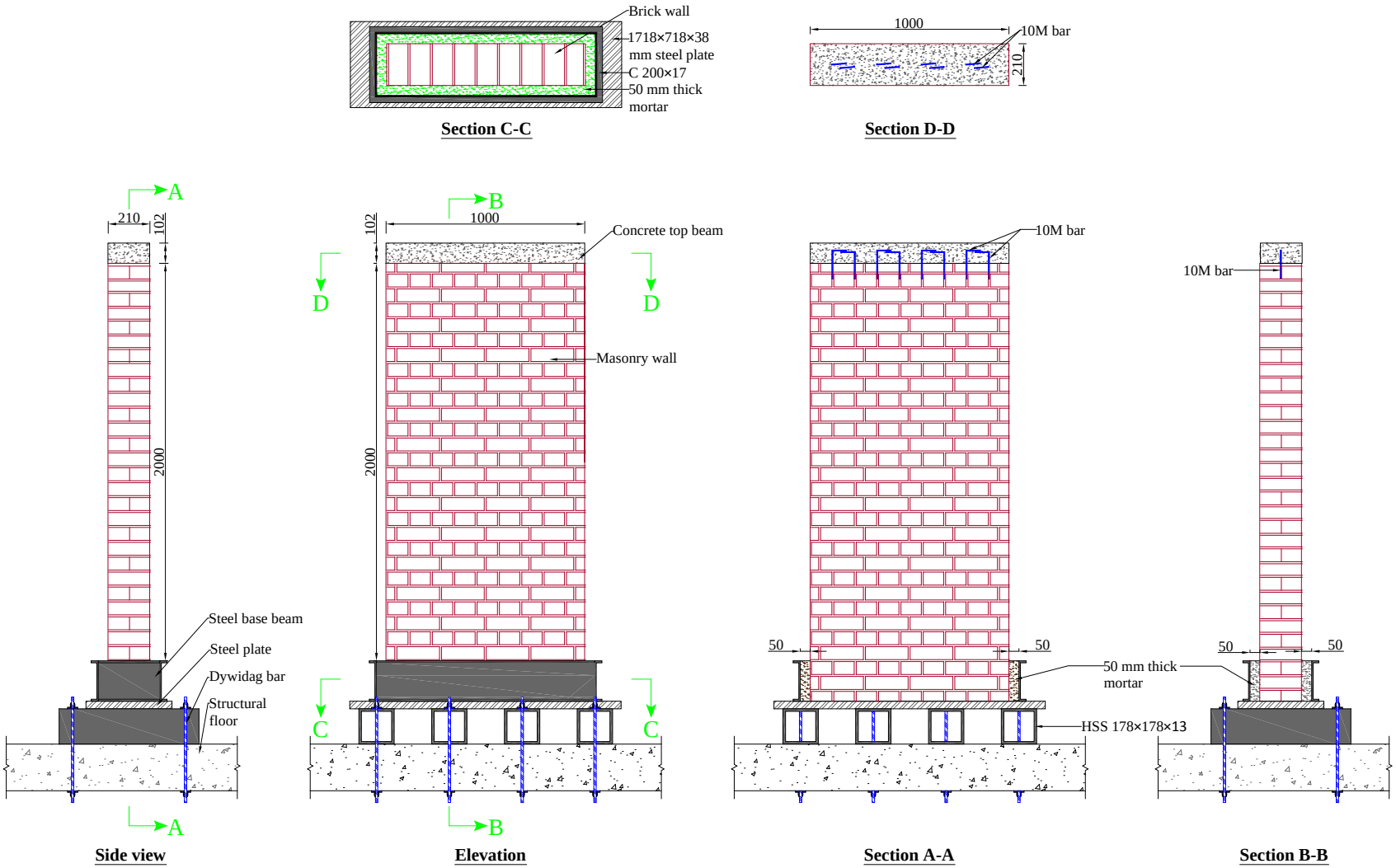

Figure 7: Details of Wall-3

(a) Side view **(b) Front view**

Figure 8: Photos of Wall-1

The following sections describe different parts of the test specimens.

3.1.1 Steel base beam

Each of the masonry walls was cast on a base beam. The beam was made of four C 200×17 sections welded together at the corners to make a formwork as can be seen in Figure 9. The formwork was welded to a 1718×718×38 mm steel plate. The space between the masonry wall and the beam was filled with 50 mm thick mortar. The beam was set over four HSS 178×178×13 sections which were tensioned to the structural floor using high strength dywidag bars.

(a) Side view of steel base beam **(b) Top view of steel base beam**

Figure 9: Detail of base beam

3.1.2 Masonry wall

Solid old clay brick units and typical soft mortar were used to build the test specimens to represent historic and old masonry walls. All the three walls were built of two wythes thick of solid clay brick units as can be seen in Figure 8. The brick units were laid as four courses of stretchers and then one course of header to represent the masonry walls of a parliament building in Ottawa. Typical soft mortar without a colour pigment, with the ratio of 1:3:9 (white Portland cement: hydrated lime type SA: sand) by volume was used. 10 mm thick mortar joints were provided in between the brick units. Typical details of masonry walls can be seen in Figure 10. The actual dimensions of the brick masonry walls after casting are presented in Table 2. The material properties of brick units, mortar and masonry prisms are presented in Table 3.

(a) Casting of wall **(b) Masonry wall without top concrete beam**

Figure 10: Typical detail of brick masonry wall

Table 2: Actual dimensions of masonry walls

Specimen designation	Height, *h* (mm)	Width, *a* (mm)	Thickness, *b* (mm)
Wall-1	1000	1040	218
Wall-2	1500	1018	212
Wall-3	2000	1015	220

Table 3: Properties of masonry walls

Specimen designation	Air content of mortar (%)	Compressive strength of masonry prism, f'_m (MPa)	Compressive strength of brick unit (MPa)	Compressive strength of mortar (MPa)
Wall-1	11.4	6.73	34.04	2.50
Wall-2	7.00	7.96		2.73
Wall-3	15.00	7.87		3.55

3.1.3 Concrete top beam

A concrete beam having a height of 102 mm and width of 210 mm was cast at the top of each masonry wall to provide a level surface as can be seen in Figure 8.

The beams were cast using concrete having a ratio of 1:3:9 (white Portland cement : hydrated lime type SA : sand) by volume. 10M steel bars were used to provide anchorage between the wall and concrete beam as can be seen in Figure 10. Concrete cylinder compressive strength tests of the top beams were conducted following the specifications of ASTM C 39 / C 39M-9 standard specifications *(ASTM 2009).* Table 4 summarizes the 28^{th} day average compressive strength of the top beams of the walls.

Table 4: 28 day compressive strength of top beam

Specimen designation	28 day compressive strength (MPa) of top beam
Wall-1	41
Wall-2	36
Wall-3	43

3.2 Casting of masonry walls

The brick masonry wall test specimens of this research program were built and tested at the University of Manitoba's W.R. McQuade Structural Laboratory. The sand, lime and cement were mixed using a mixture for the homogeneous mixing of mortar. After mixing the mortar, the air content of the freshly mixed mortar mix was determined by conducting the air entrainment test of mortar mix by using the specifications of ASTM C231/C231M-03 *(ASTM 2003)*. The test results of air entrainment test are presented in Table 3. In total, 12 mortar cubes having dimensions of 50 × 50 × 50 mm were built for each wall specimen to conduct the future compressive strength tests. The tests were conducted by using the specifications of ASTM C109/C109M -07 *(ASTM 2007-a)* to determine the compressive strength of the mortar. The 28 day compressive strengths of the mortar cubes are given in Table 3.

At first a layer of 50 mm thick mortar was placed over the base beam. Then the brick units were laid with 10 mm thick mortar joints. All the three walls were built of two wythes thick of solid clay brick units as can be seen in Figure 8. The brick units were laid as four courses of stretchers and then one course of header to represent the masonry walls

of a parliament building in Ottawa. 10M steel bars were placed at top layers of brick to provide anchorage between the wall and concrete beam. After completion of the building of each wall, the wall was covered with burlap and cured for 7 days.

After 14 days, the formwork for the top beam was prepared following by the casting of the concrete top beam. Figure 11 shows different stages of casting of a masonry wall.

(a) Mixing of mortar

(b) Mortar mix

(c) Air entrainment test

(d) Making mortar cubes

(e) Placing of first brick layer

(f) Wall without concrete top beam

(g) Casting of concrete top beam

(h) Complete wall

Figure 11: Different stages of masonry wall construction

3.3 Test setup

Schematic details of a typical test setup for the experimental program are shown in Figure 12. The bottom face of the wall was fixed to the laboratory strong floor through a steel base beam. The steel base beam was tensioned to the laboratory strong floor using eight high strength dywidag bars. A 102 × 210 mm concrete beam was cast at top of each masonry walls to provide a level surface for the application of horizontal and vertical loads. The W250×73 steel load beam was supported by two W130×28 steel columns. The columns were cross braced with several C380×50 and HSS102×102×4.8 sections. The W130×28 steel columns were tensioned to the structural floor using high strength dywidag bars. A325 structural bolts were used in all the bolted connections.

A hydraulic jack and an actuator were used to apply the static vertical and horizontal loads on the walls. A steel beam made of C380×50 sections was placed under the hydraulic jack concentric to the wall. The vertical loads were applied at two points at a distance of one third length of corresponding wall using two sets of steel rollers. A 355 mm deep steel beam was placed at the top of the concrete beam to transfer and uniformly distribute the vertical loads to the masonry wall. A photograph of the typical test setup for the experimental program can be seen in Figure 13.

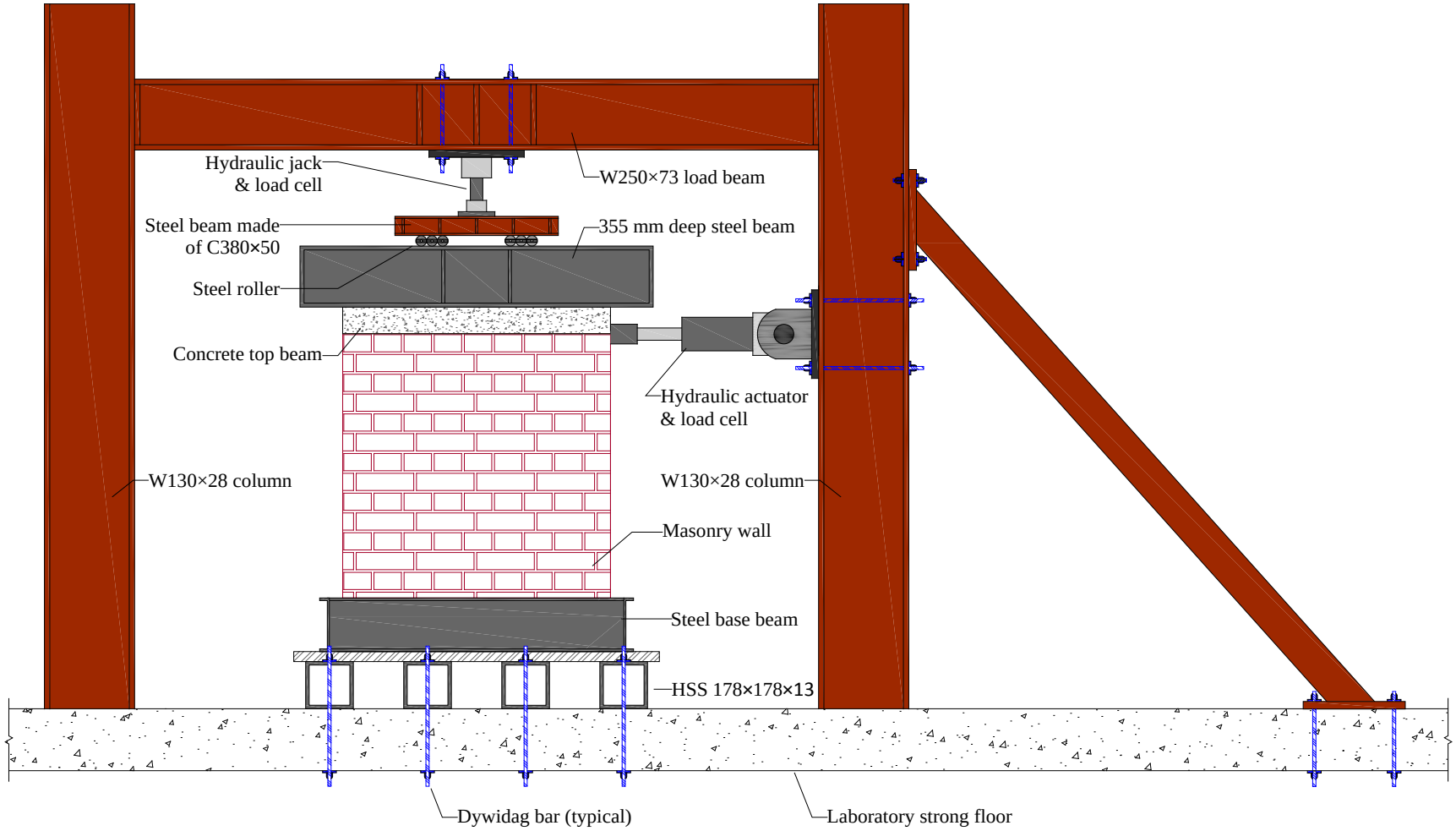

Figure 12: Schematic detail of typical test setup

Figure 13: Photograph of typical test setup

3.4 Detail of instrumentations

Different types of instruments were installed to record the experimental data including the magnitude of vertical and horizontal loads, horizontal and vertical deflections of the wall. The following sections describe the test setup for each of the test specimens.

3.4.1 Wall-1

Two vertical (LVDT-NV and LVDT-SV) and eight horizontal Linear Variable Displacement Transducers (LVDT-N1, LVDT-N2, LVDT-N3, LVDT-N4, LVDT-N5, LVDT-S1, LVDT-S2 and LVDT-S3) were installed in Wall-1 to record the horizontal

and vertical displacements of the masonry wall as shown in Figure 14. Horizontal LVDTs were placed at the top and at one third heights of both the north and south faces of the wall to record horizontal displacements and observe the displacement profile of the wall. One horizontal LVDT (LVDT-N5) was positioned at the base of the steel beam to record the movement of the steel base with respect to the laboratory strong floor. Two vertical LVDTs (LVDT-NV and LVDT-SV) were placed at a distance of 100 mm from north and south edges of the wall to record its vertical displacements.

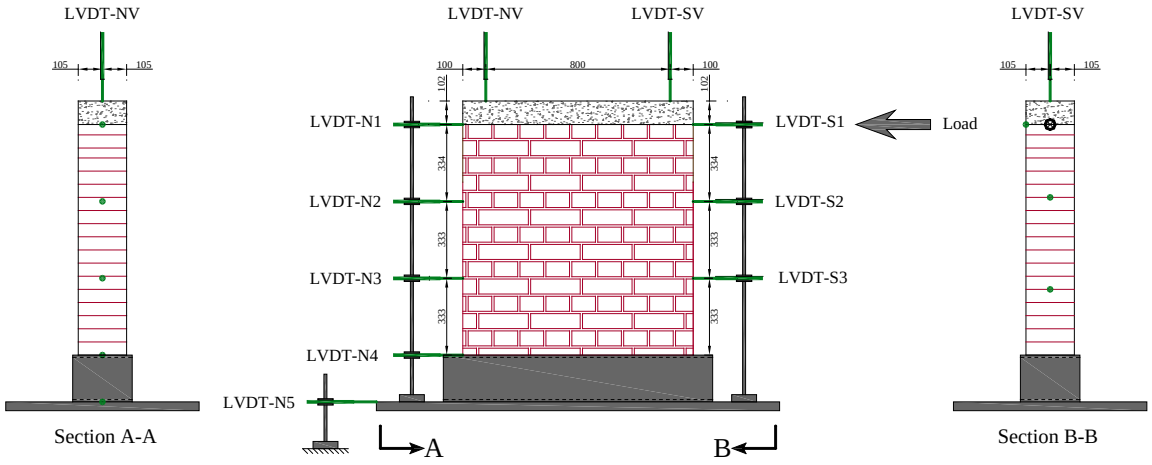

Figure 14: Instrument setup of wall-1

3.4.2 Wall-2

Two vertical (LVDT-NV and LVDT-SV) and seven horizontal Linear Variable Displacement Transducers (LVDT-N1, LVDT-N2, LVDT-N3, LVDT-N4, LVDT-N5, LVDT-S1, LVDT-S2 and LVDT-S3) were installed in Wall-2 to record the horizontal and vertical displacements of the masonry wall as shown in Figure 15. Horizontal LVDTs were placed at the top and at one third heights of both north and south faces of the wall to

record horizontal displacements and observe the displacement profile of the wall. One horizontal LVDT was positioned at the base of the steel beam relative to laboratory strong floor to record movement of the steel base with respect to the laboratory strong floor. Two vertical LVDTs were placed at distance of 100 mm from north and south edges of the wall to record vertical displacements.

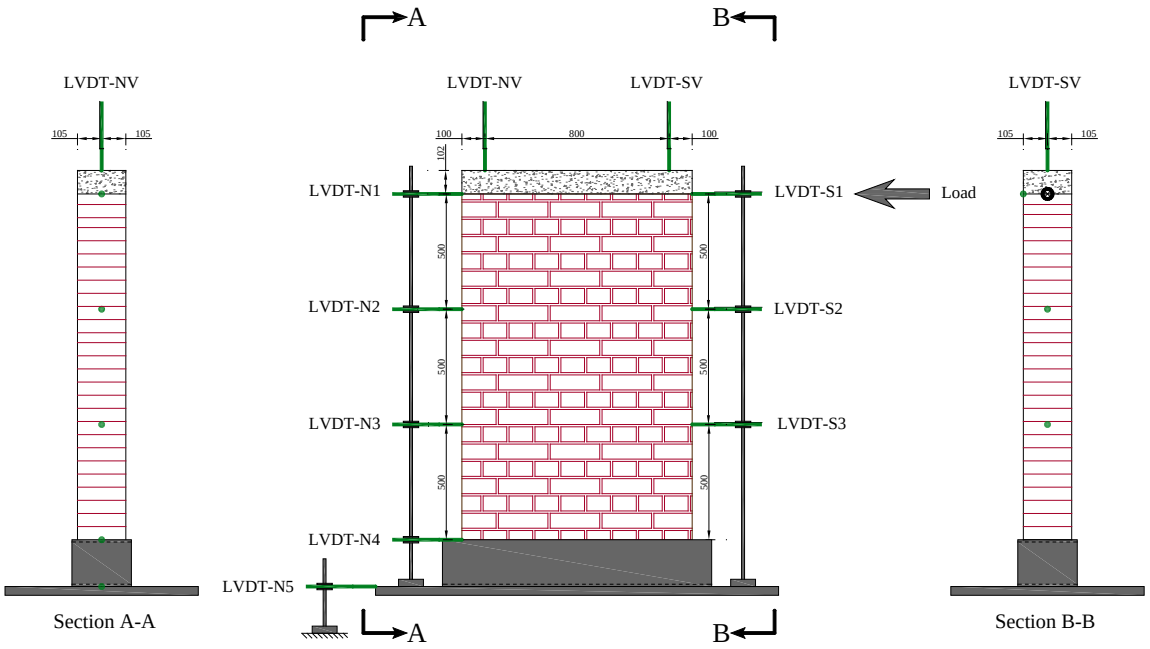

Figure 15: Instrument setup of wall-2

3.4.3 Wall-3

Two vertical (LVDT-NV and LVDT-SV) and six horizontal Linear Variable Displacement Transducers (LVDT-N1, LVDT-N2, LVDT-S1, LVDT-S2, LVDT-M1, and LVDT-M2) were installed in Wall-3 to record the horizontal and vertical displacement values of the masonry wall as shown in Figure 16. Horizontal LVDTs were

placed at the top and at one third heights of both north and south faces of the wall to record horizontal displacements and observe the displacement profile of the wall.

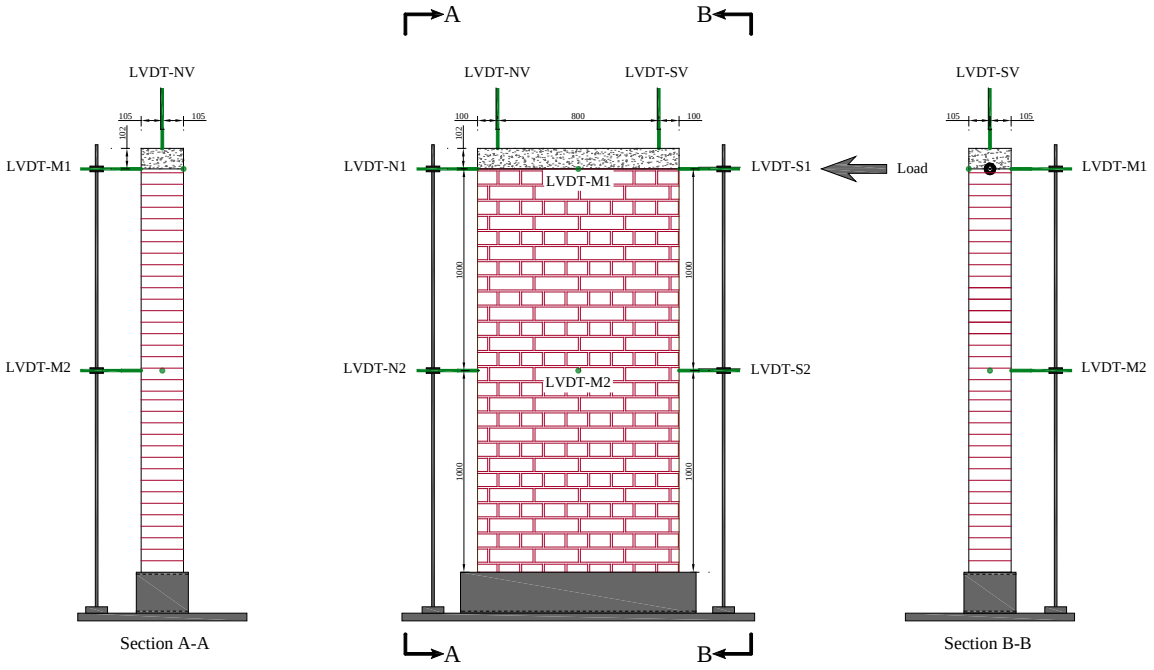

Figure 16: Instrument setup of wall-3

3.5 Test procedure

A constant two point vertical load was applied on each of the unreinforced masonry walls using a hydraulic jack as can be seen in Figure 12. The amount of vertical stress for the walls was decided to be 0.2 MPa which lead to 46 kN of a concentrated load or 23 kN each of two point vertical loads. The in-plane lateral load was applied at the walls using a hydraulic actuator in displacement control mode to avoid the sudden collapse of the masonry walls. Lateral load was applied to the masonry wall until the first crack was

visible by bare eyes. Once the first crack was visible, the lateral load was removed and the crack pattern of the corresponding wall was examined.

Chapter 4

Experimental Results

The experimental test results of three unreinforced masonry walls are presented in this chapter. The test results presented in the following sections are the lateral load versus lateral displacement, lateral load versus vertical displacement, and crack patterns on the masonry walls.

4.1 Test results of Wall-1

4.1.1 Lateral load versus lateral displacement

The lateral load versus lateral displacement profiles, until the initiation of first visible crack on Wall-1, at the locations of LVDT-S1, LVDT-S2, LVDT-S3, LVDT-N1, LVDT-N2, LVDT-N3, LVDT-N4 and LVDT-N5 can be seen in Figure 17, Figure 18, Figure 19, Figure 20, Figure 21, Figure 22, Figure 23 and Figure 24 respectively. During the test, the first flexural crack was visible by bare eyes at around 22 kN of horizontal load. It is seen

from Figure 17, and Figure 20 that the slope of the load-displacement profile changed at around 22 kN of horizontal load which indicates the initiation of first flexural crack in the masonry wall. The first flexural crack was observed at the bottom of the south face of the wall at the mortar bed joint. LVDT-S2 was not functioning properly until 21 kN and yielded unusual reading as shown in Figure 18.

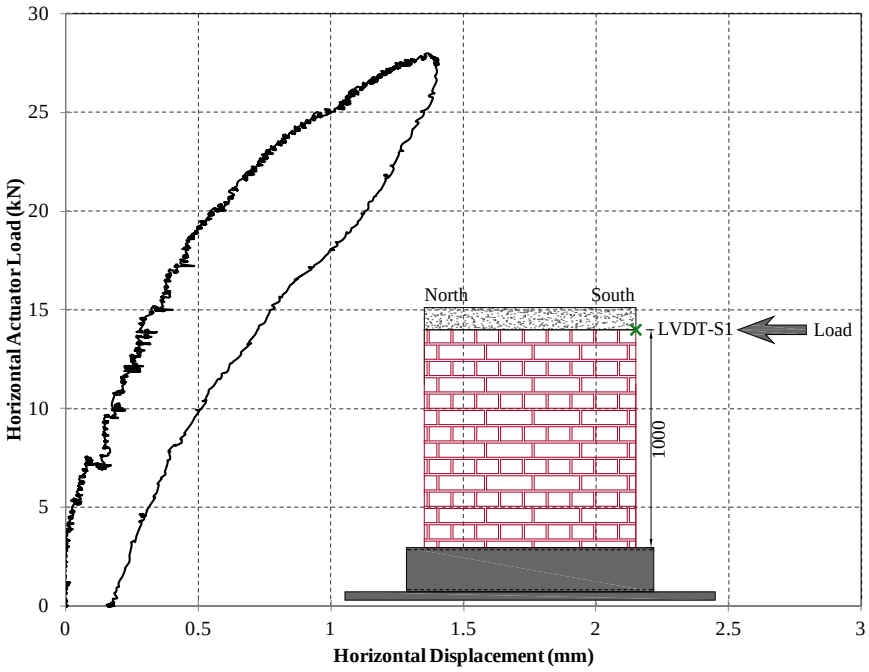

Figure 17: Horizontal load versus horizontal displacement profile at location of LVDT-S1 of Wall-1

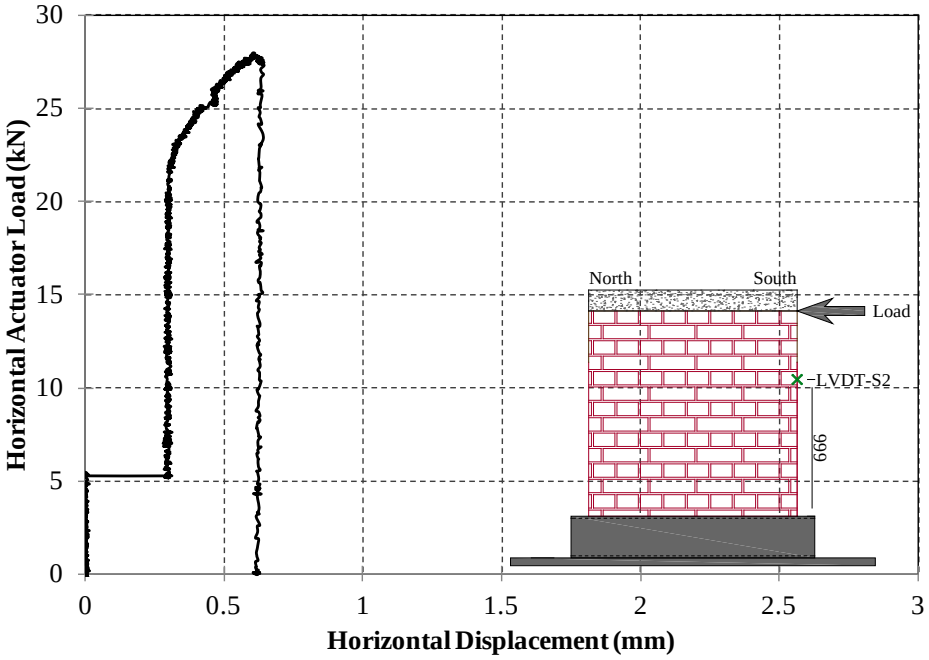

Figure 18: Horizontal load versus horizontal displacement profile at location of LVDT-S2 of Wall-1

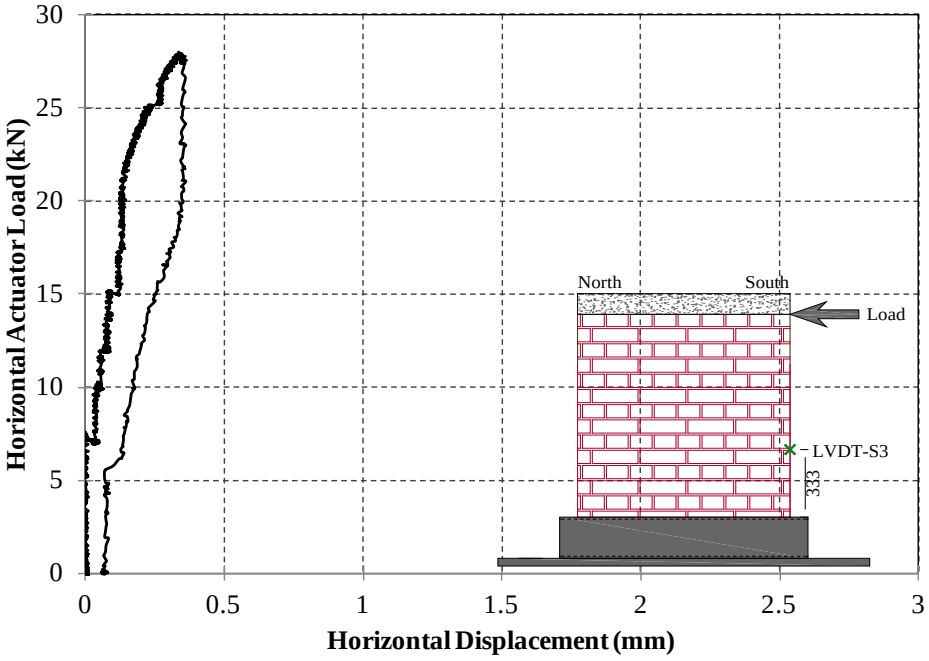

Figure 19: Horizontal load versus horizontal displacement profile at location of LVDT-S3 of Wall-1

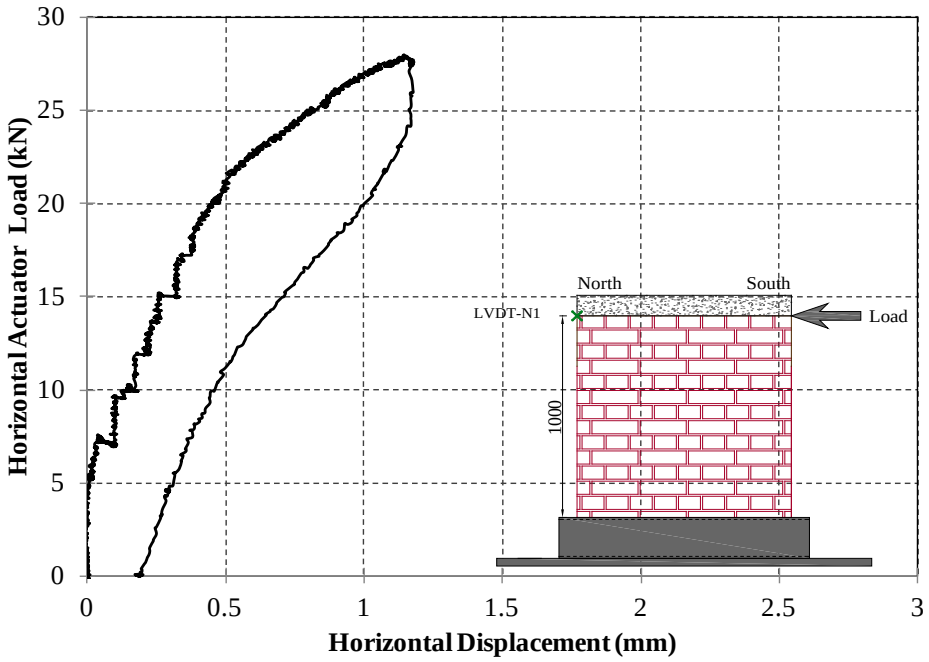

Figure 20: Horizontal load versus horizontal displacement profile at location of LVDT-N1 of Wall-1

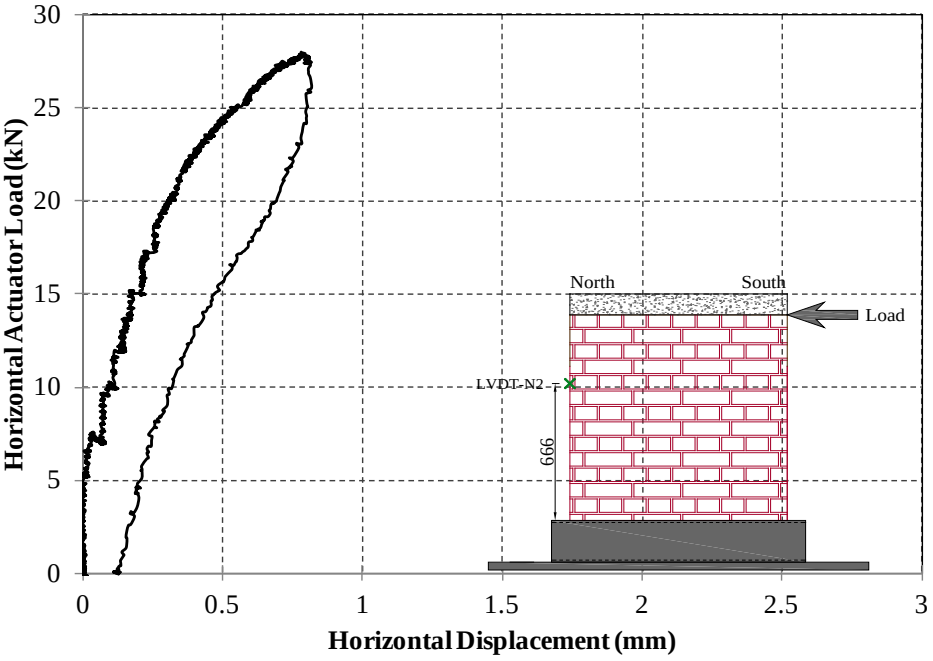

Figure 21: Horizontal load versus horizontal displacement profile at location of LVDT-N2 of Wall-1

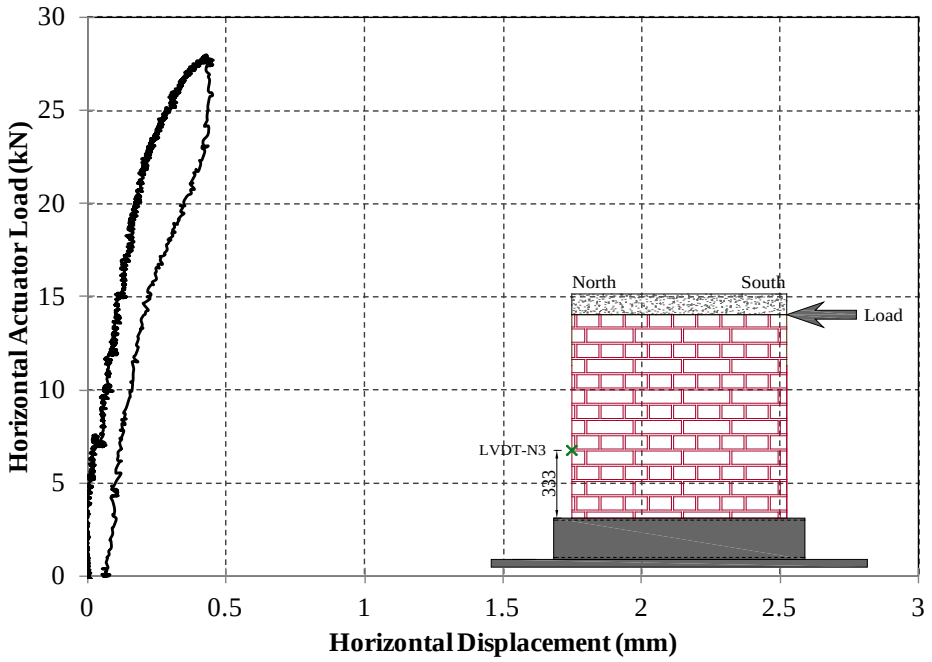

Figure 22: Horizontal load versus horizontal displacement profile at location of LVDT-N3 of Wall-1

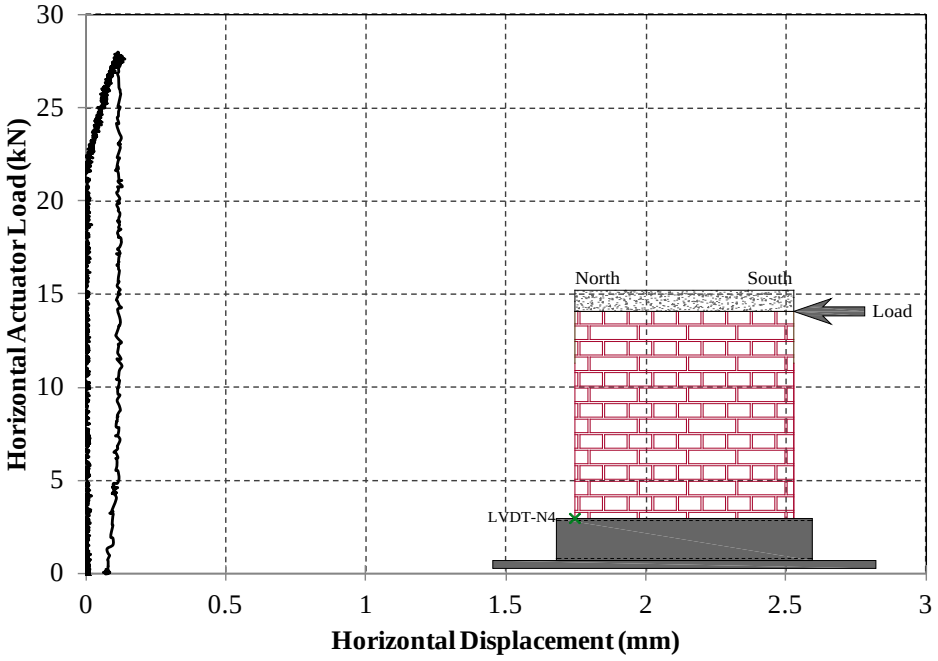

Figure 23: Horizontal load versus horizontal displacement profile at location of LVDT-N4 of Wall-1

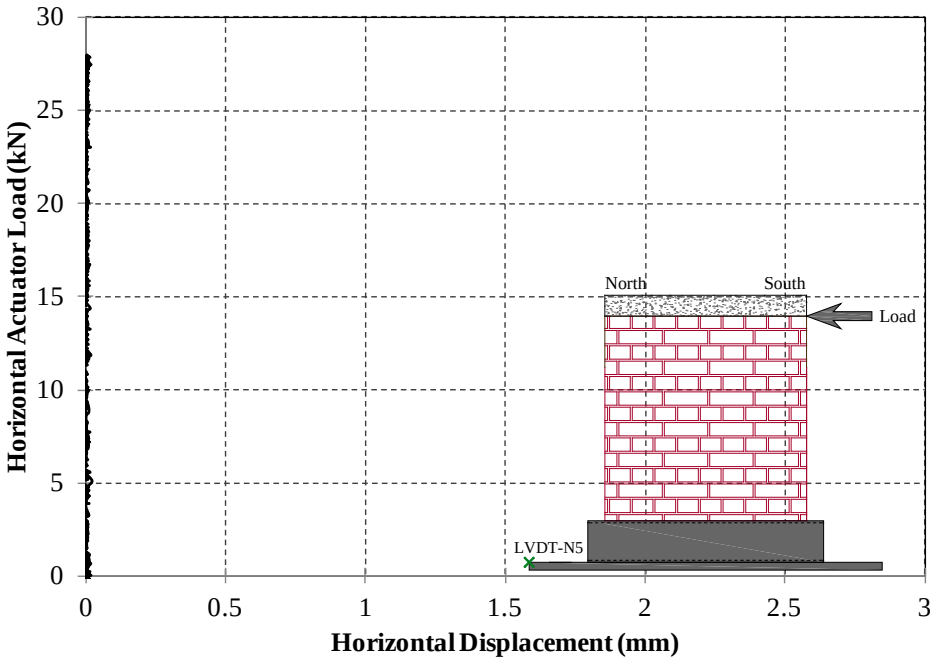

Figure 24: Horizontal load versus horizontal displacement profile at location of LVDT-N5 of Wall-1

Figure 25 shows the displacement profiles of north and south faces of the wall at different horizontal loads (5 kN, 10 kN, 15 kN, 20 kN and 25 kN) until initiation of first visible crack. The dotted and solid lines indicate the horizontal displacement of north and south faces of the wall respectively. As can be seen in Figure 25, horizontal displacement of the bottom of the wall (at location LVDT-N4) was either zero or negligible. The horizontal displacements of the wall increased with the increment of the height from the bottom of the wall, and with the increment of the magnitude of horizontal load. The south face of the wall (the horizontal load application face) deflected more than the north face of the wall. The maximum deflections recorded at initiation of the first visible crack (at 22 kN) at the top and bottom of the wall were around 0.99 mm (at location of LVDT-S1) and 0.05 mm (at location of LVDT-N4) respectively.

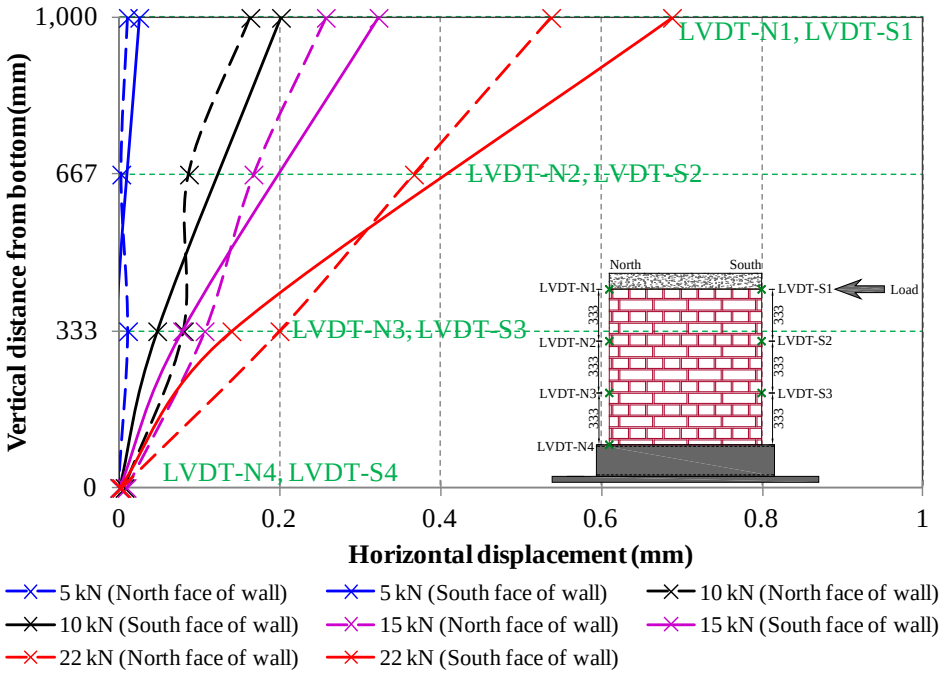

Figure 25: Displacement profiles of north and south faces of Wall-1

Comparison of horizontal load versus horizontal displacements until the initiation of first visible crack at different locations of horizontal LVDTs of wall-1 can be seen in Figure 26.

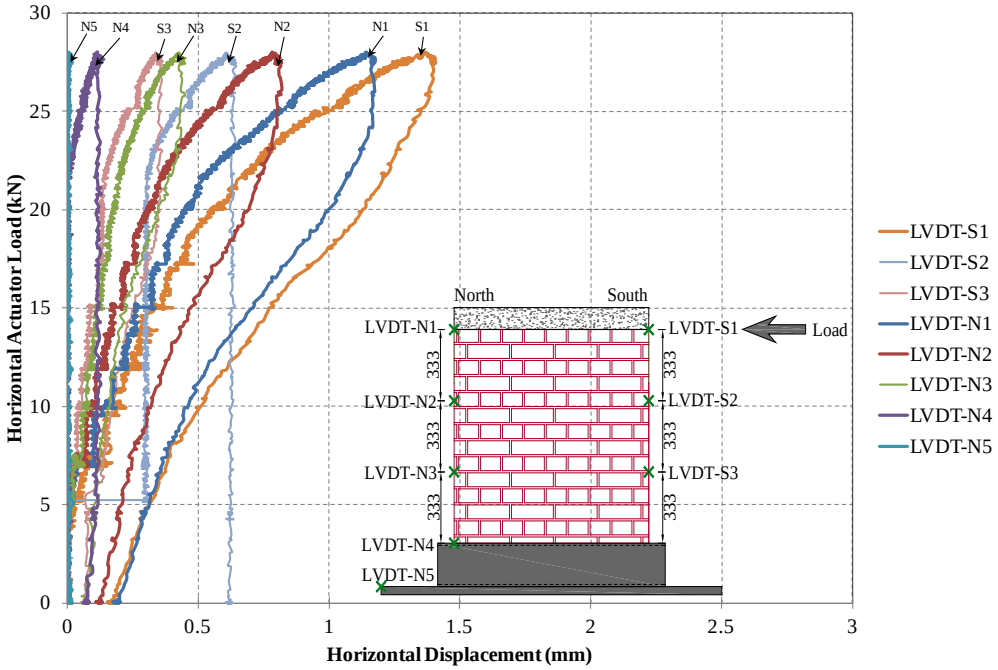

Figure 26: Lateral load versus horizontal displacement behaviour of Wall-1

4.1.2 Lateral load versus vertical displacement

The lateral load versus vertical displacement profiles, until the initiation of first visible crack on Wall-1, at the location of LVDT-SV and LVDT-NV can be seen in Figure 27 and Figure 28 respectively. As can be seen in Figure 27 the south side (tension side) of the wall moved upward and the maximum upward movement at initiation of first crack is around 0.1 mm. According to Figure 28, the north side (compression side) of the wall moved downward and the maximum downward movement at initiation of first crack was around 0.65 mm.

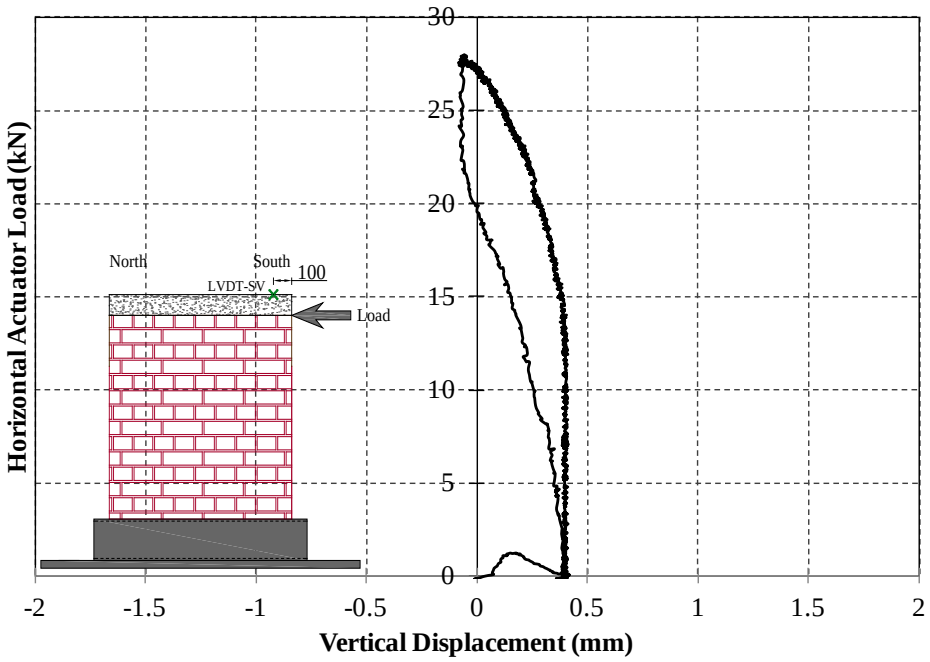

Figure 27: Horizontal load versus vertical displacement profile at location of LVDT-SV of Wall-1

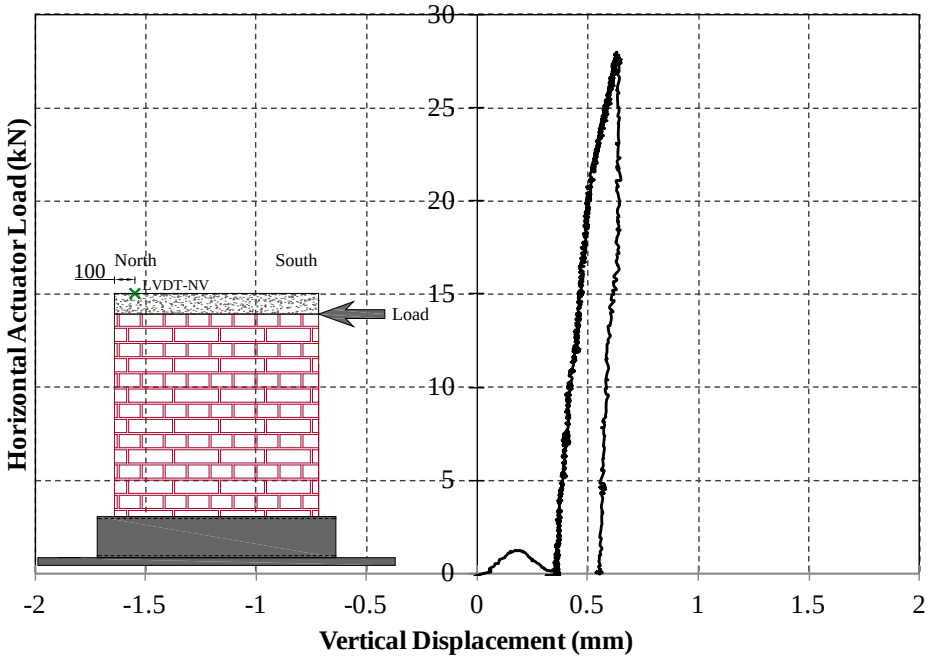

Figure 28: Horizontal load versus vertical displacement profile at location of LVDT-NV of Wall-1

4.1.3 Deflection profile of wall

The deflection profile of Wall-1 at initiation of first crack at 22 kN can be seen in Figure 29. The wall in grey colour indicate the position of the wall before application of load and the red line indicates the deflected profile of the wall at initiation of first crack. The locations of the LVDTs can be seen as green crosses.

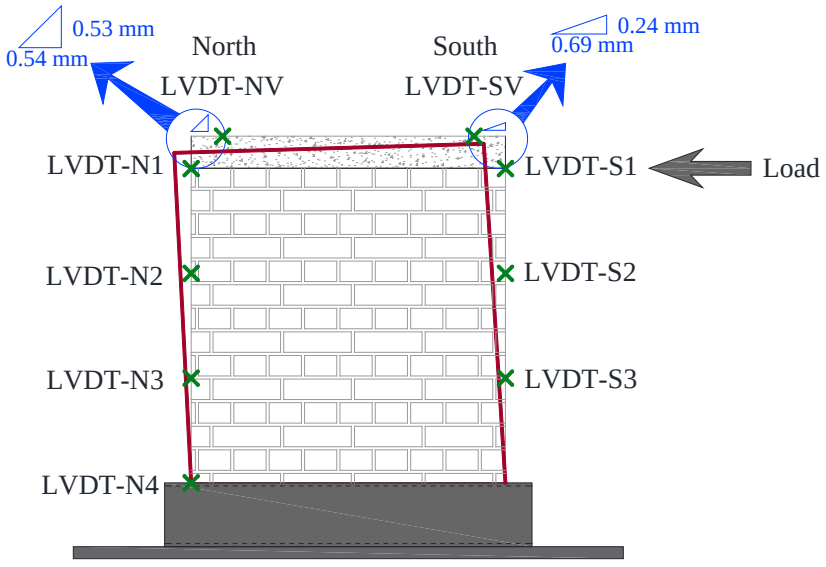

LVDT	Deflection (mm)
LVDT-N1	0.54
LVDT-N2	0.37
LVDT-N3	0.21
LVDT-N4	0.01
LVDT-NV	0.53

LVDT	Deflection (mm)
LVDT-S1	0.69
LVDT-S2	0.30
LVDT-S3	0.14
LVDT-SV	0.24

Figure 29: Deflection profile of Wall-1 at initiation of first crack

4.1.4 Crack pattern

The observed crack patterns of wall-1 can be seen in Figure 30. The first horizontal flexural crack was visible at the mortar of the support bed joint at the south side (tension

side) at around 22 kN of horizontal load. With the increment of the horizontal load, a shear crack initiated and propagated from North-bottom corner to South-top direction as can be seen in Figure 30(b). Simultaneously the flexural crack propagated from south to north direction and widened at support bed joint.

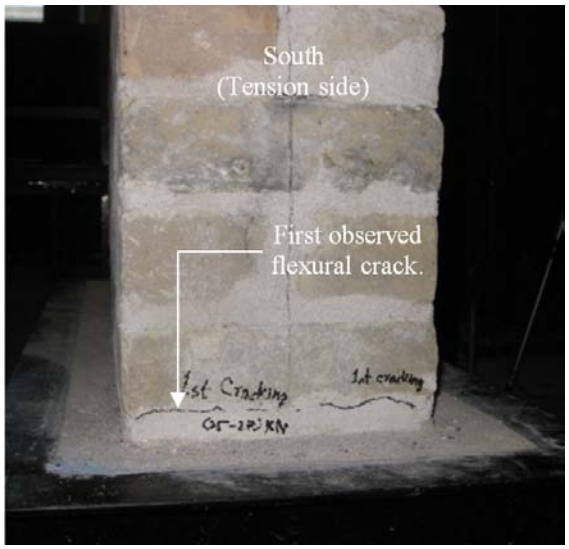

(a) South side view

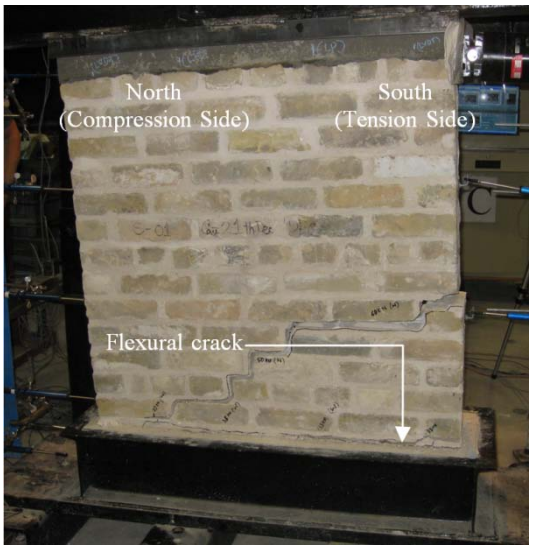

(b) Front view

Figure 30: Flexural crack pattern at bottom of Wall-1

4.2 Test results of Wall-2

4.2.1 Lateral load versus lateral displacement

The lateral load versus lateral displacement profiles, until the initiation of first visible crack on Wall-2, at the locations of LVDT-S1, LVDT-S2, LVDT-S3, LVDT-N1, LVDT-N2, LVDT-N3, LVDT-N4 and LVDT-N5 can be seen in Figure 31, Figure 32, Figure 33, Figure 34, Figure 35, Figure 36, Figure 37, and Figure 38 respectively. During the test,

the first flexural crack was visible by bare eyes at around 15 kN of horizontal load. The first flexural crack was observed to be at the bottom of the south face of the wall at the mortar bed joint. As seen from Figure 31 and Figure 37, the maximum deflection recorded at initiation of the first visible crack (at 15 kN) at the top and bottom of the wall were around 0.96 mm (at location of LVDT-S1) and 0 mm (at location of LVDT-N4) respectively. From Figure 31, Figure 32, Figure 34 and Figure 35 it is seen that the recorded deflections are either zero or negligible until around13 kN. This indicates that the LVDTs were not able to read the small deflections. More sensitive deflection measuring instruments, such as LMTs (Linear Motion Tandem Transducer), might be used to record such small deflection.

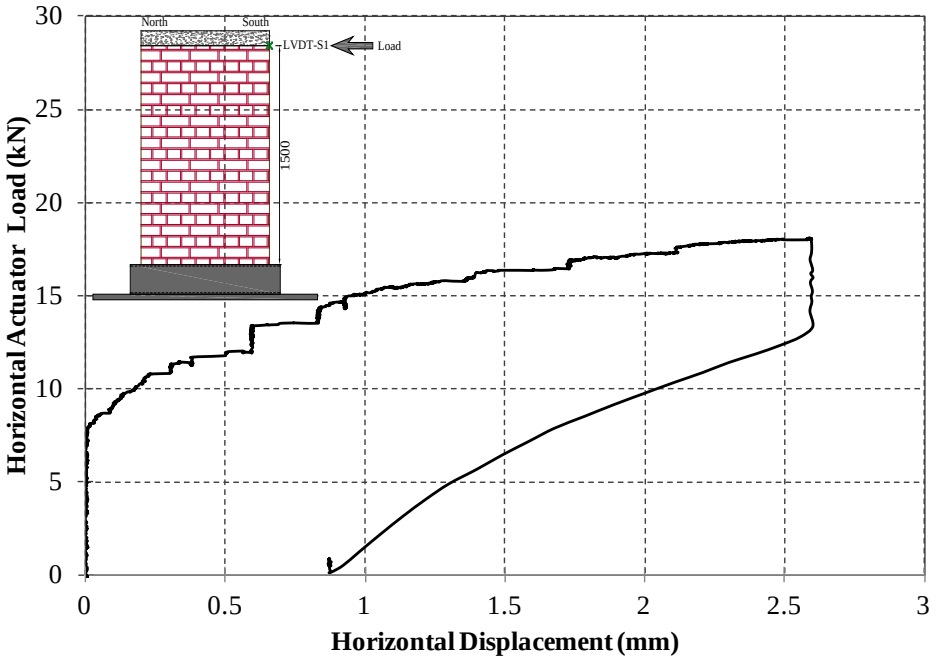

Figure 31: Horizontal load versus horizontal displacement profile at location of LVDT-S1 of Wall-2

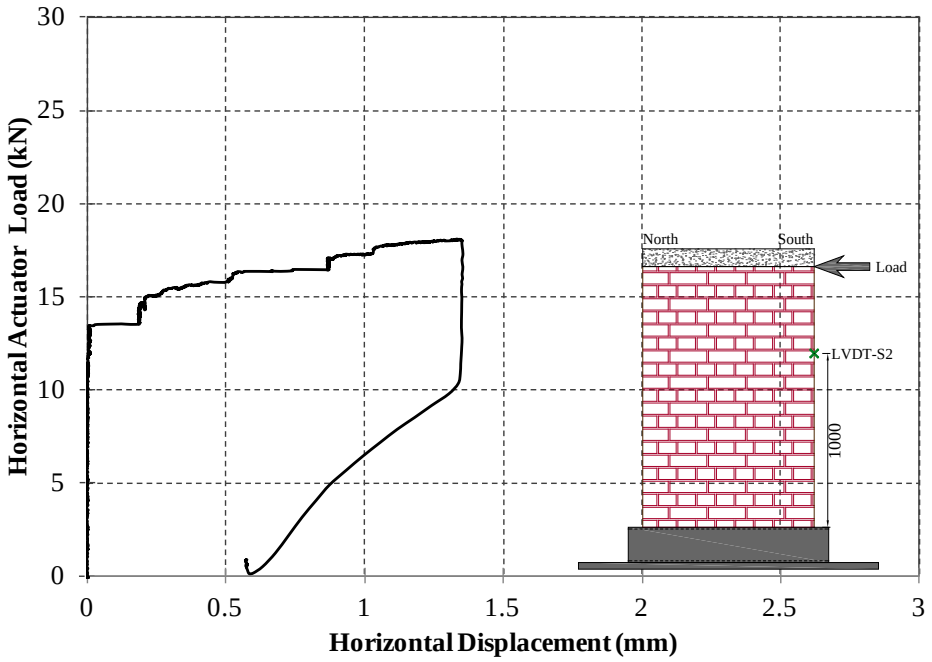

Figure 32: Horizontal load versus horizontal displacement profile at location of LVDT-S2 of Wall-2

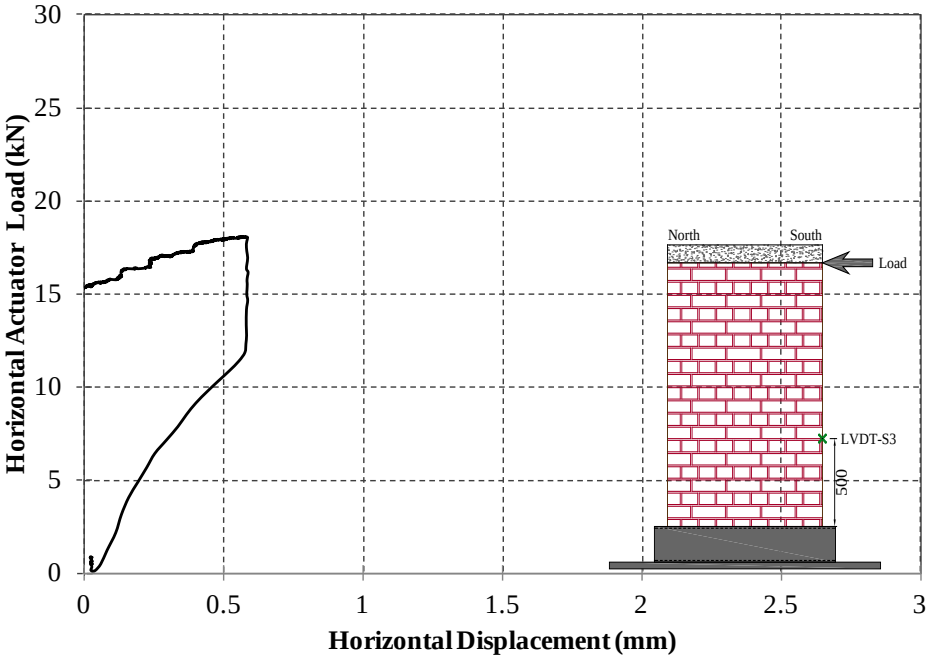

Figure 33: Horizontal load versus horizontal displacement profile at location of LVDT-S3 of Wall-2

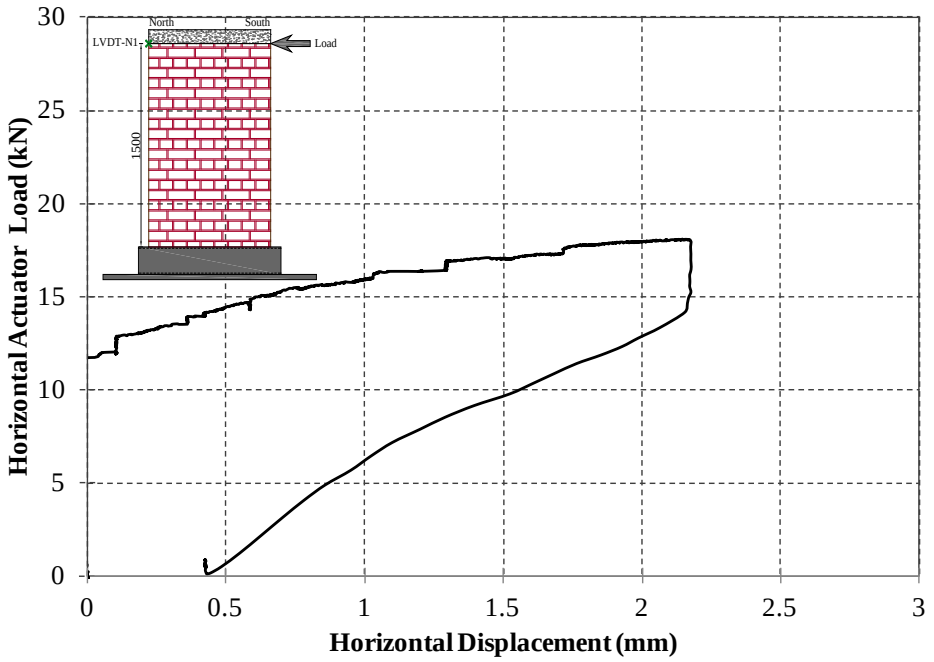

Figure 34: Horizontal load versus horizontal displacement profile at location of LVDT-N1 of Wall-2

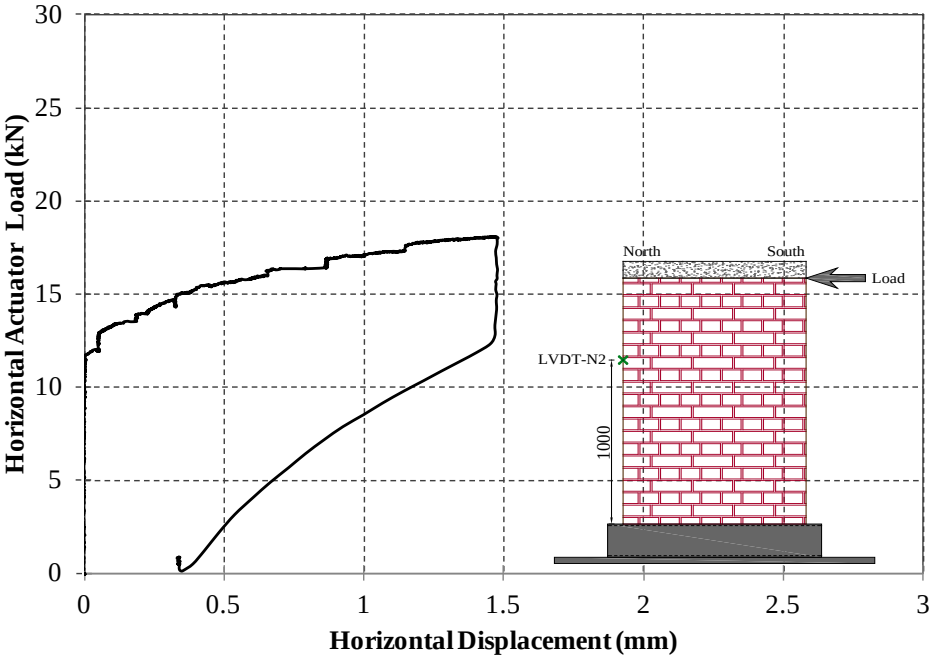

Figure 35: Horizontal load versus horizontal displacement profile at location of LVDT-N2 of Wall-2

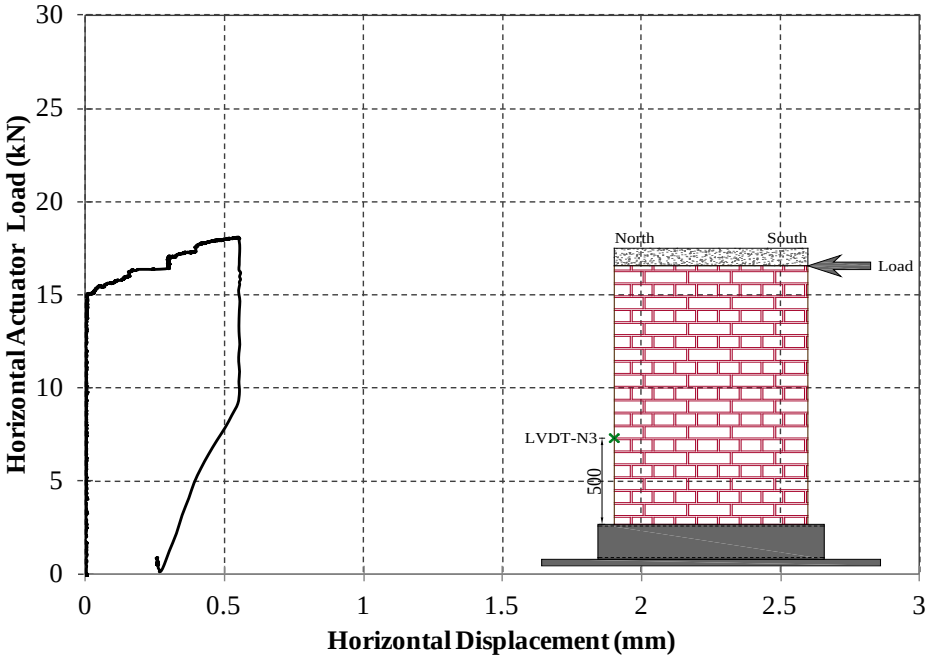

Figure 36: Horizontal load versus horizontal displacement profile at location of LVDT-N3 of Wall-2

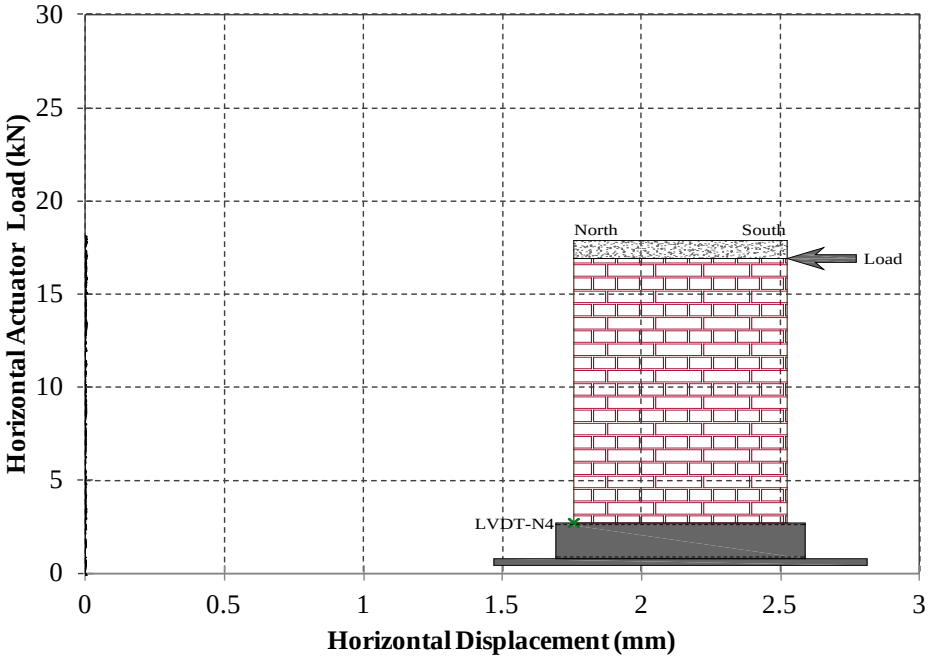

Figure 37: Horizontal load versus horizontal displacement profile at location of LVDT-N4 of Wall-2

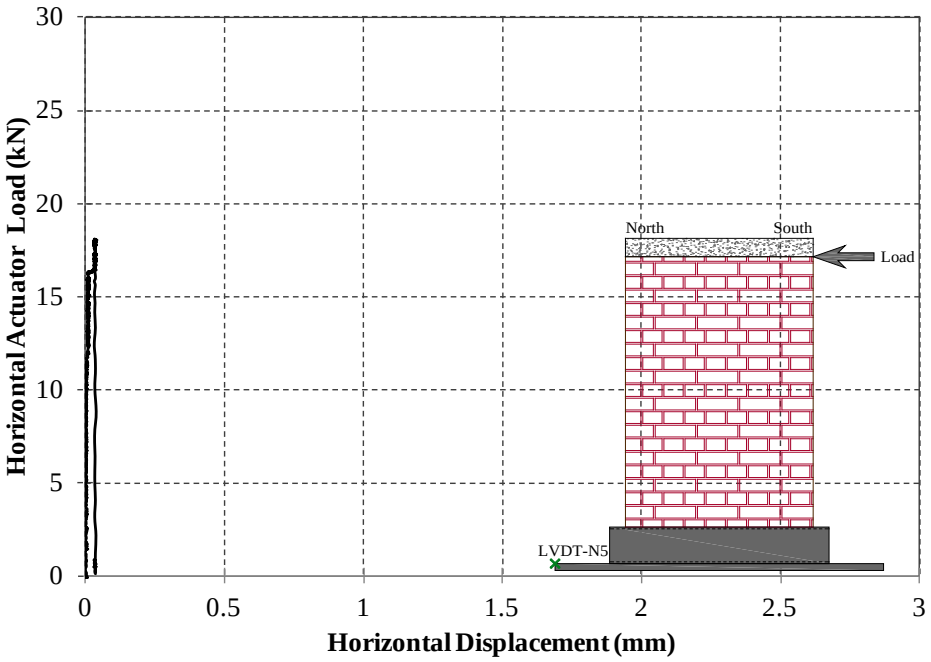

Figure 38: Horizontal load versus horizontal displacement profile at location of LVDT-N5 of Wall-2

Figure 39 shows the displacement profiles of north and south faces of the wall at initiation of the first visible crack (at 15 kN). There was zero or negligible horizontal displacement of the bottom of the wall (at location LVDT-N4). The deflection of the wall increased with the height from the bottom of the wall. The south face of the wall (the horizontal load application face) deflected more than the north face of the wall. The maximum deflection recorded at initiation of the first visible crack at the top and bottom of the wall were around 0.96 mm (at location of LVDT-S1) and 0 mm (at location of LVDT-N4) respectively.

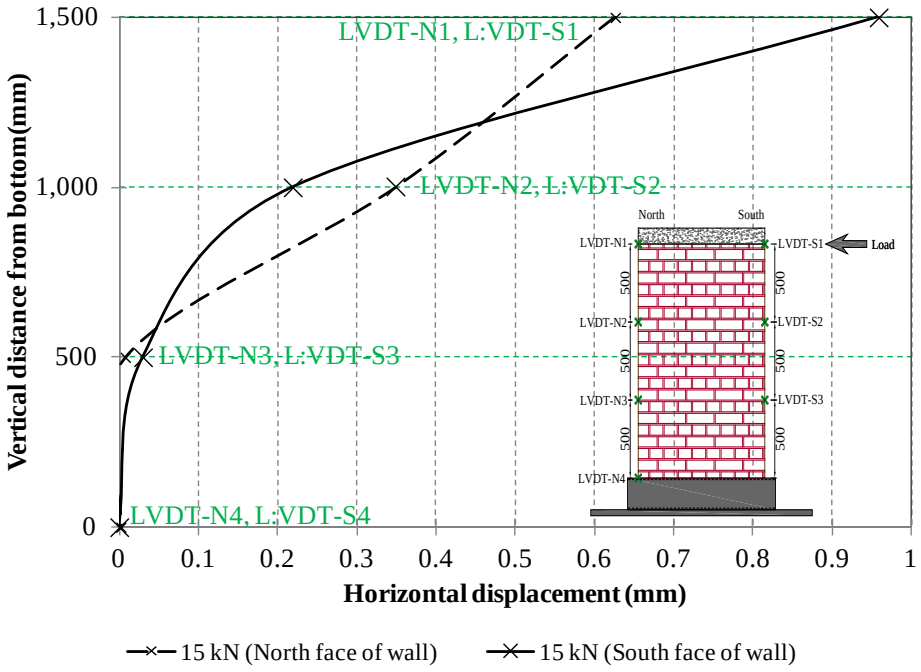

Figure 39: Displacement profiles of north and south faces of Wall-2

4.2.2 Lateral load versus vertical displacement

The lateral load versus vertical deflection profiles, until the initiation of first visible crack on Wall-2, at the locations of LVDT-NV and LVDT-SV can be seen in Figure 40 and Figure 41 respectively. As shown in Figure 40, the north side (compression side) of the wall moved downward and the maximum downward movement at initiation of first crack was around 1.5 mm. According to Figure 41, the south side (tension side) of the wall also moved downward and the maximum downward movement at initiation of first crack was around 0.75 mm.

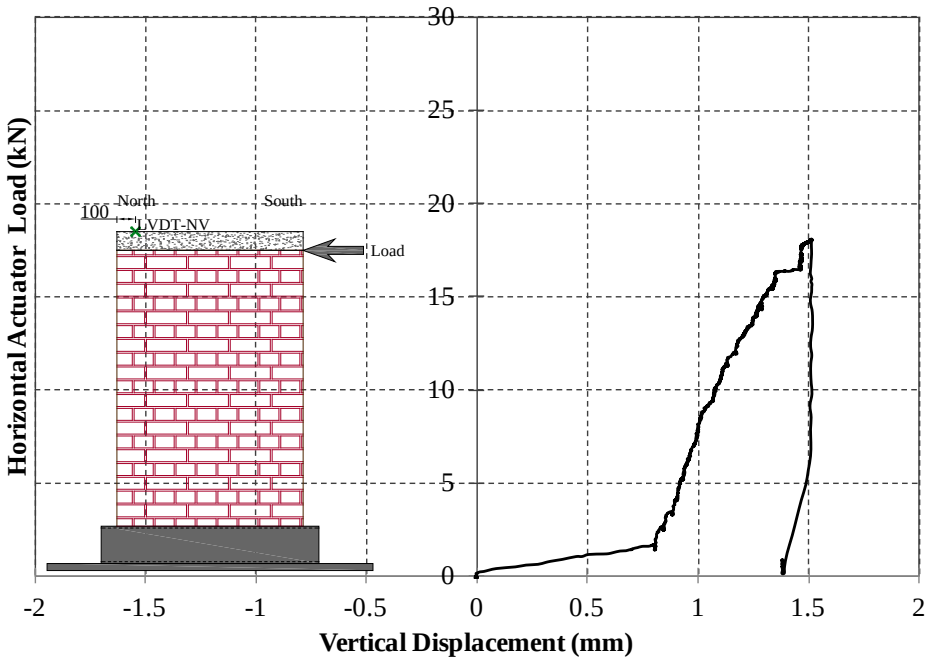

Figure 40: Horizontal load versus vertical displacement profile at location of LVDT-NV of Wall-2

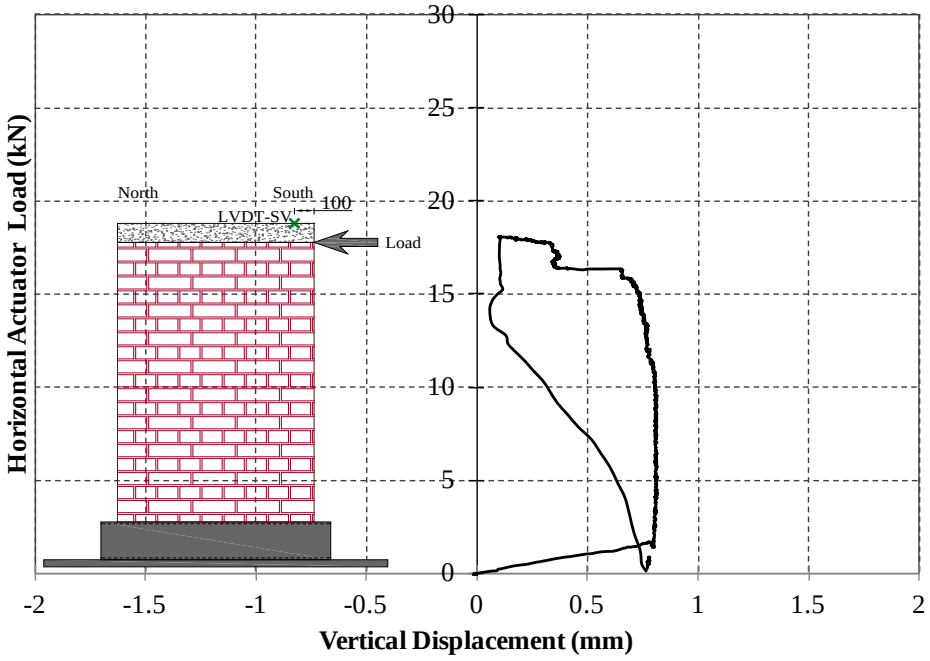

Figure 41: Horizontal load versus vertical displacement profile at location of LVDT–SV of Wall-2

4.2.3 Deflection profile of wall

The deflection profile of Wall-2 at initiation of first crack at 15 kN can be seen in Figure 42. The wall in grey colour indicate the position of the wall before application of load and the red line indicates the deflected profile of the wall at initiation of first crack. The locations of the LVDTs can be seen as green crosses.

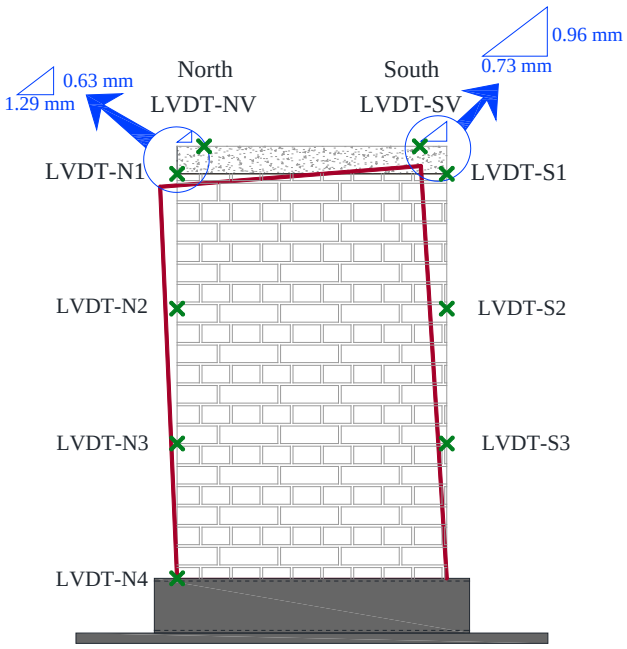

LVDT	Deflection (mm)
LVDT-N1	0.63
LVDT-N2	0.36
LVDT-N3	0.01
LVDT-N4	0.00
LVDT-NV	1.29

LVDT	Deflection (mm)
LVDT-S1	0.96
LVDT-S2	0.25
LVDT-S3	0.00
LVDT-SV	0.73

Figure 42: Deflection profile of Wall-2 at initiation of first crack

4.2.4 Crack pattern

The observed crack patterns of Wall-2 can be seen in Figure 43. The first horizontal flexural crack was visible in the mortar of the support bed joint at the south side (tension side) of the wall at around 15 kN of horizontal load. With increment of the horizontal load, the flexural crack propagated from south to north direction and widened at the support bed joint.

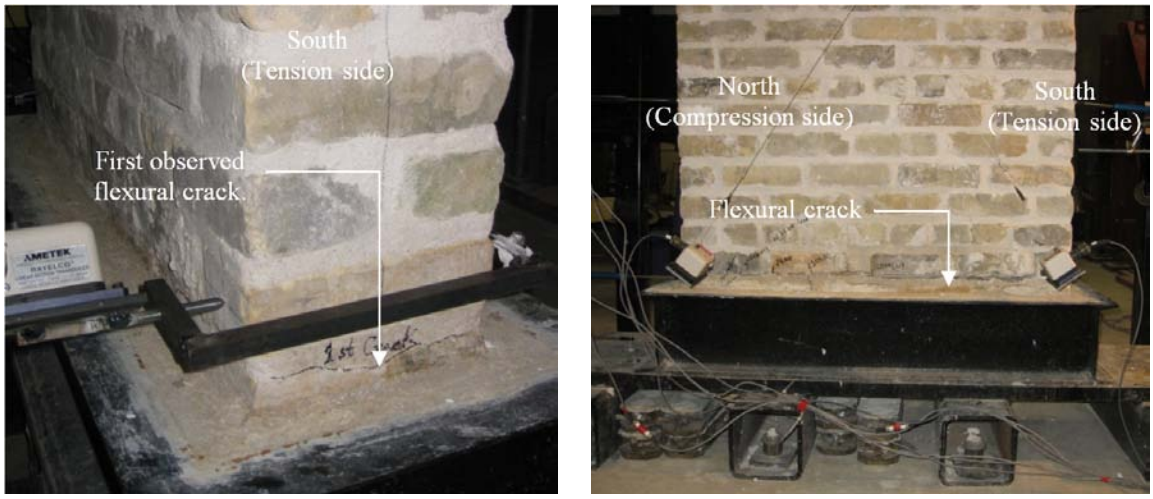

(a) South side view **(b) Front view**

Figure 43: Flexural crack pattern at bottom of Wall-2

4.3 Test results of Wall-3

4.3.1 Lateral load versus lateral displacement

The lateral load versus lateral displacement profiles, until the initiation of the first visible crack on Wall-3, at the locations of LVDT-S1, LVDT-S2, LVDT-N1, LVDT-N2, LVDT-

M1 and LVDT-M2 can be seen in Figure 44, Figure 45, Figure 46, Figure 47, Figure 48, and Figure 49 respectively. During the test, the first flexural crack was visible by bare eyes at 12.42 kN of horizontal load. The first flexural crack was observed to be at the bottom of the south face of the wall at the mortar bed joint. As seen from Figure 44 and Figure 46, the maximum deflection recorded at initiation of the first visible crack (at 12.42 kN of lateral load) at top of south and north faces of the wall were around 0.48 mm (at location of LVDT-S1) and 1 mm (at location of LVDT-N1) respectively. The vertical LVDTs (LVDT-NV and LVDT-SV) did not work properly during the test and that is why the test data recorded by those LVDTs are not presented in this report.

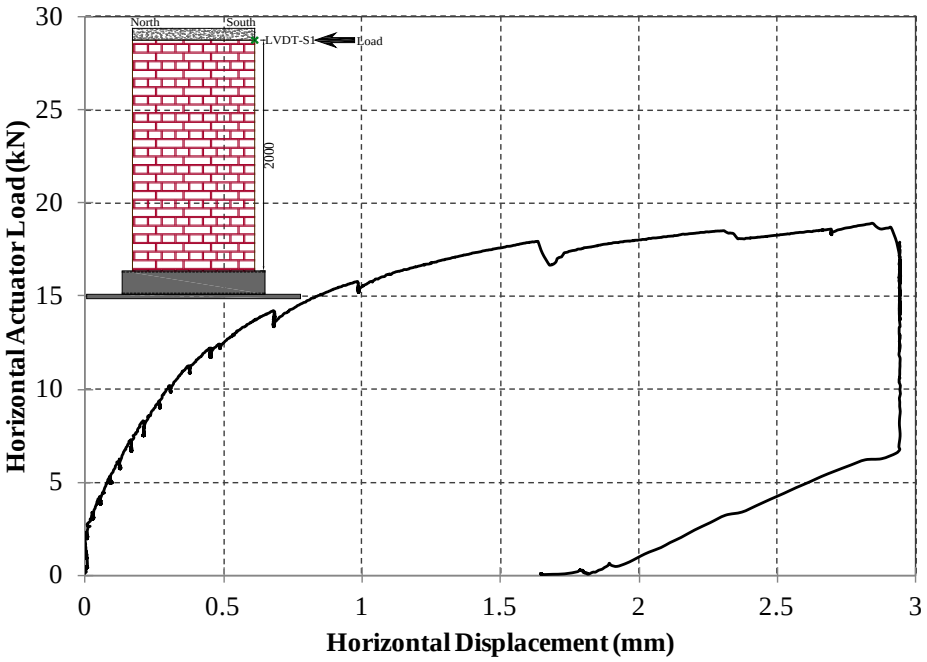

Figure 44: Horizontal load versus horizontal displacement profile at location of LVDT-S1 of Wall-3

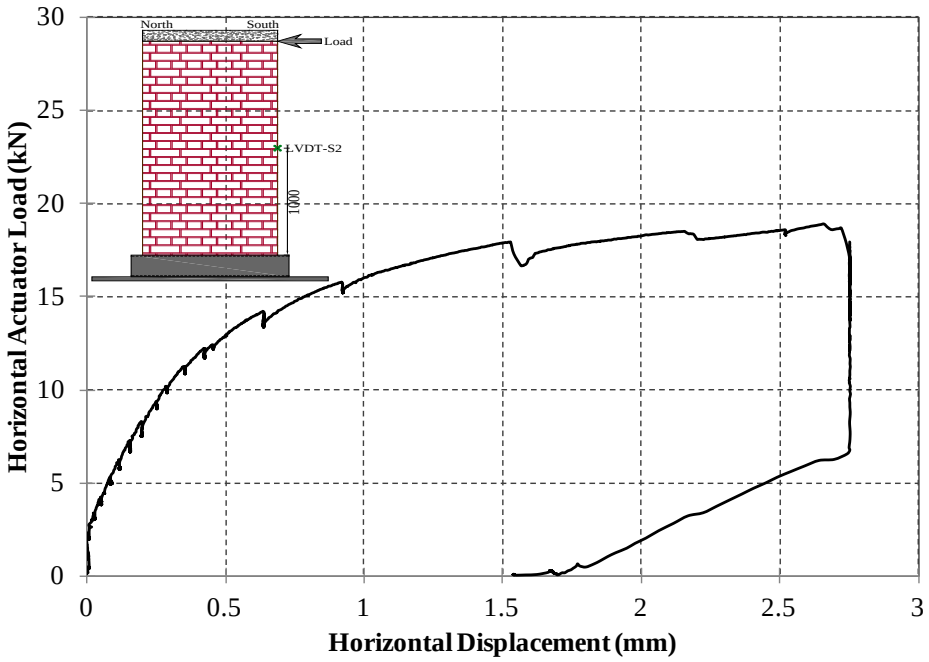

Figure 45: Horizontal load versus horizontal displacement profile at location of LVDT–S2 of Wall-3

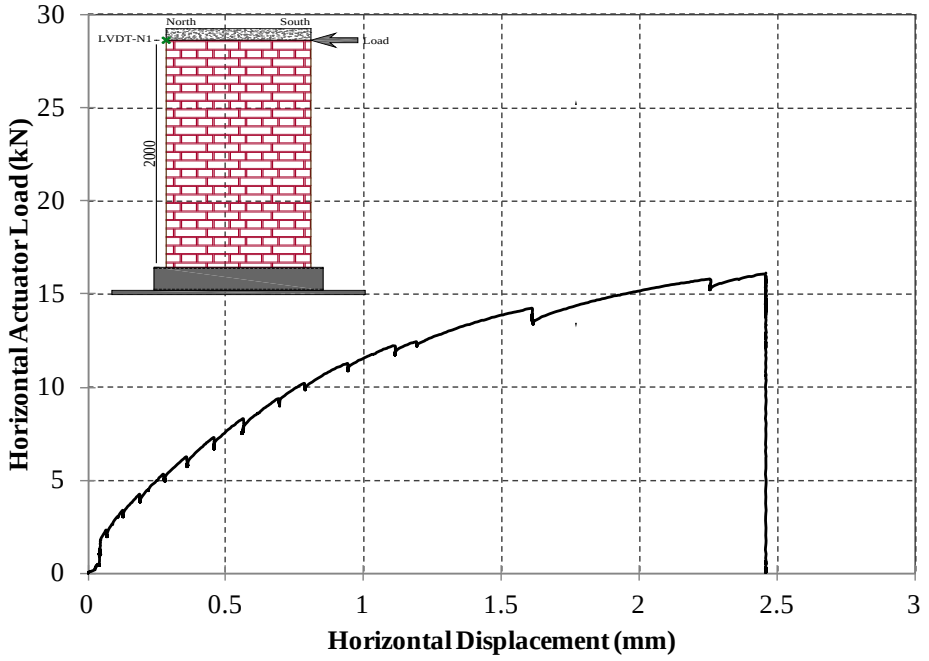

Figure 46: Horizontal load versus horizontal displacement profile at location of LVDT-N1 of Wall-3

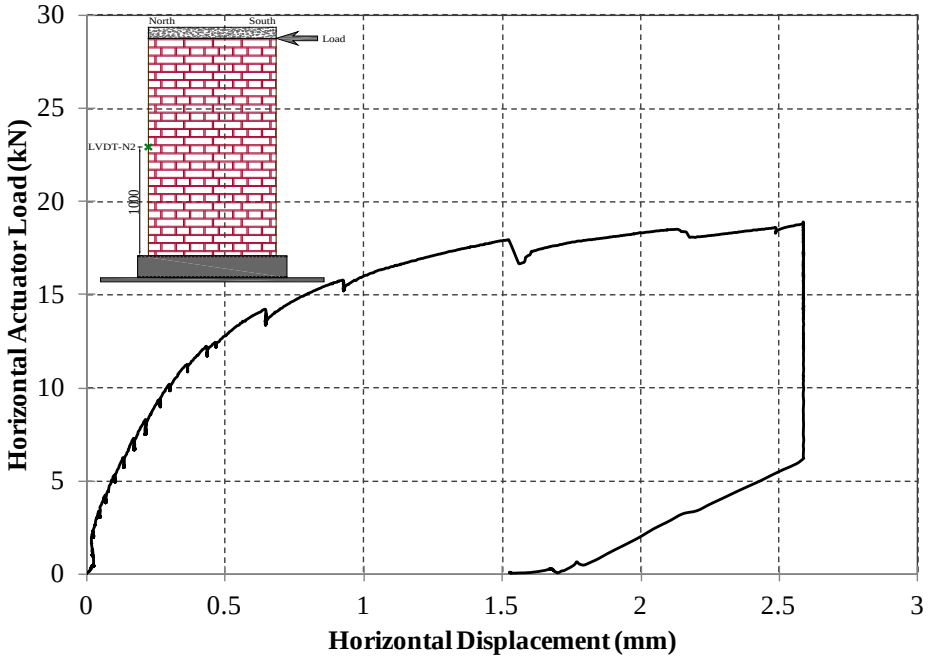

Figure 47: Horizontal load versus horizontal displacement profile at location of LVDT–N2 of Wall-3

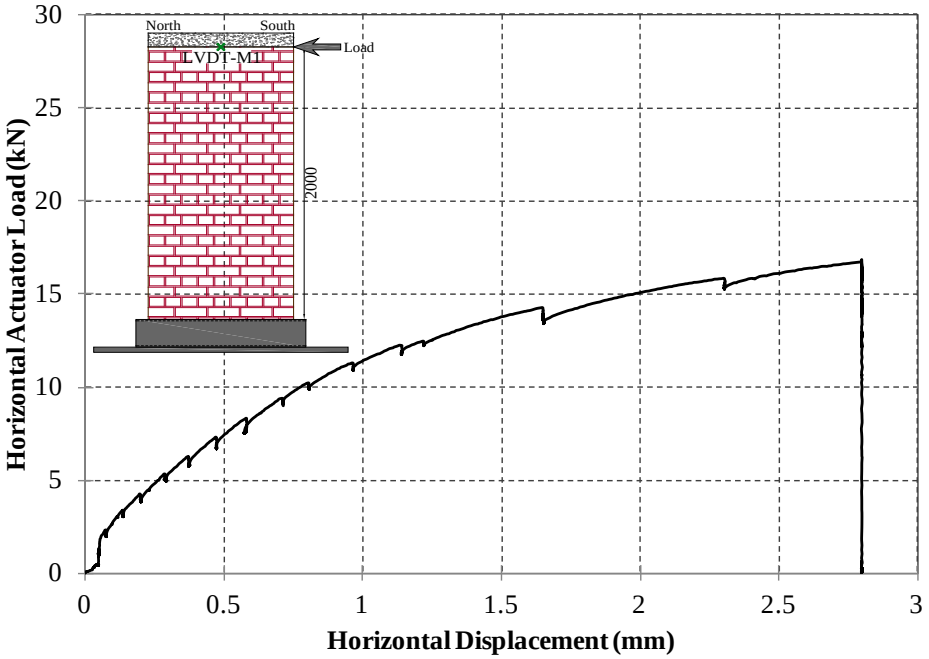

Figure 48: Horizontal load versus horizontal displacement profile at location of LVDT-M1 of Wall-3

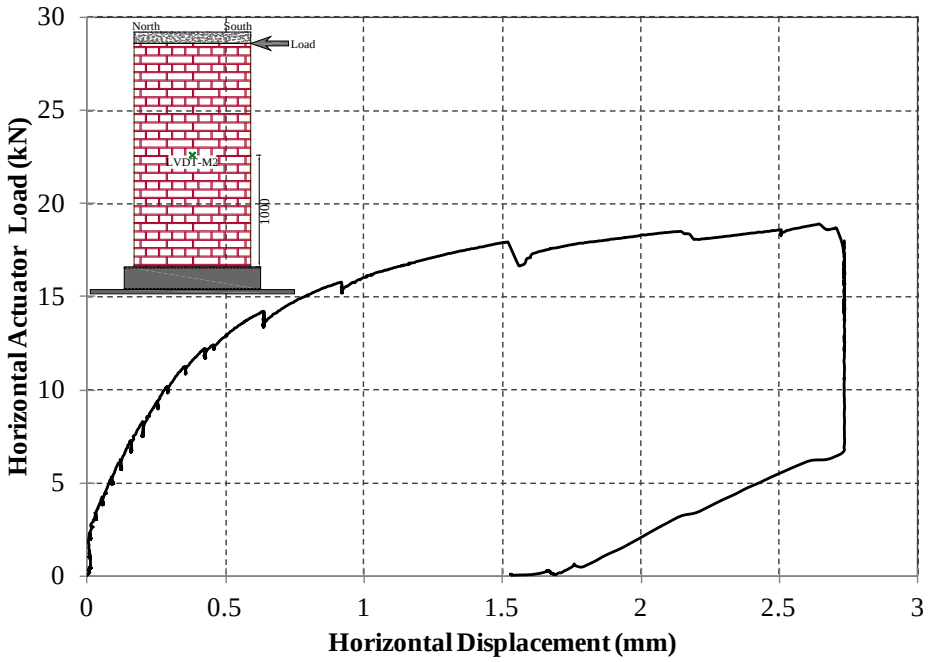

Figure 49: Horizontal load versus horizontal displacement profile at location of LVDT-M2 of Wall-3

Figure 50 shows the displacement profiles of north and south faces of the wall at initiation of the first visible crack (at 12.42 kN). There is no (or negligible) horizontal displacement of the bottom of the wall (at location LVDT-N4). The deflection of the wall increased with the increment of the height from the bottom of the wall. The north face of the wall deflected more than the south face of the wall. As seen in Figure 50, the deflections at the locations of LVDT-S1 and LVDT-S2 showed almost same deflection (0.45 mm) at initiation of first crack. As the distance from the fixed end of the wall to the location of LVDT-S1 is more than that of LVDT-S2, theoretically the deflection recorded by LVDT-S1 should be more than that of LVDT-S2 at the same horizontal load. This indicates that LVDT-S1 was not functioning properly. For this reason the deflection profile of south face of Wall-3 was discarded for analysis. The maximum deflection

recorded at initiation of the first visible crack at top of the wall was around 1.2 mm (at location of LVDT-N1).

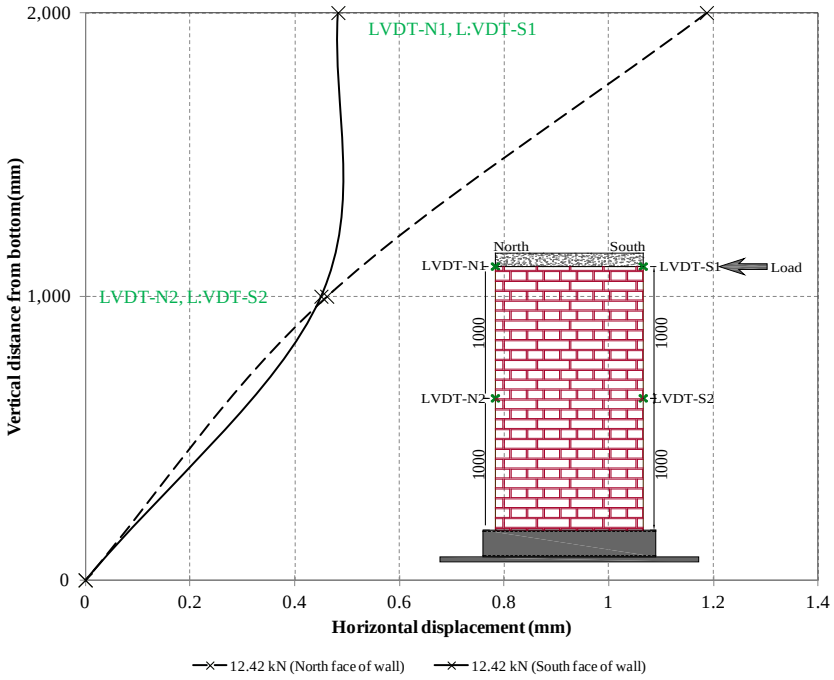

Figure 50: Displacement profiles of north and south faces of Wall-3

4.3.2 Crack pattern

The observed crack patterns of Wall-3 can be seen in Figure 51. The first horizontal flexural crack was visible in the mortar of the support bed joint at the south side (tension side) at around 12.42 kN of horizontal load. With increment of the horizontal load, the flexural crack propagated from south to north direction and widened at support bed joint.

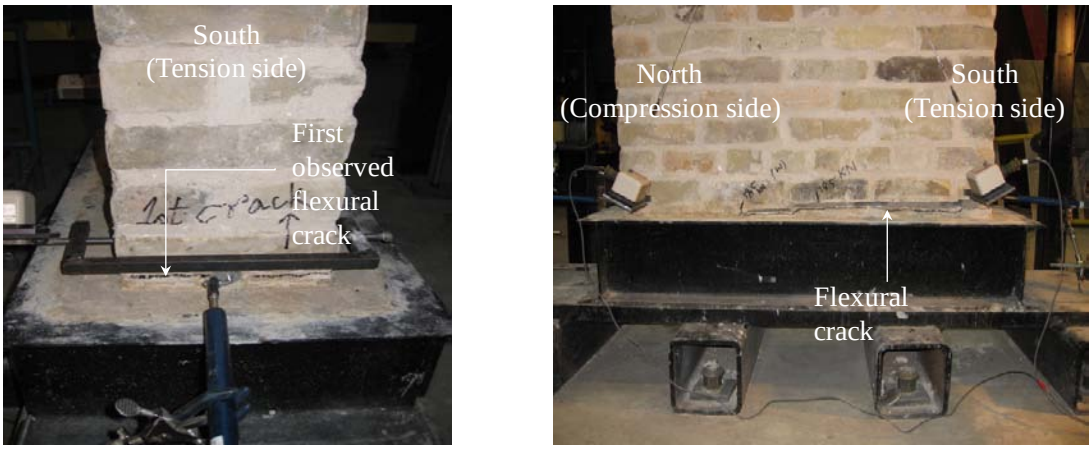

(a) South side view **(b) Front view**

Figure 51: Flexural crack pattern at bottom of Wall-3

4.4 Summary of test results

The test results of this research project are summarized in Table 5.

Table 5: Summary of test results

	Wall-1	**Wall -2**	**Wall -3**
Wall height, *h* (mm)	1000	1500	2000
Horizontal load at initiation of first crack, *P* (kN)	22	15	12.42
Maximum horizontal defection at initiation of first crack, δ (mm)	0.69	0.96	1.20
Ratio between deflections at initiation of first crack and wall heights ($\frac{\delta}{h}$)	$\frac{1}{1450}$	$\frac{1}{1563}$	$\frac{1}{1667}$
Type of first visible crack	Flexural	Flexural	Flexural
First flexural crack visible at	South (tension) side	South (tension) side	South (tension) side
First flexural crack initiated at	Support bed joint mortar	Support bed joint mortar	Support bed joint mortar
Initiation of shear crack with increment of horizontal load	Yes	No	No

Chapter 5

Data Analysis

The following sections describe the calculation of modulus of elasticity (E) and shear modulus (G) of brick masonry walls according to the CSA Standard, the Jaeger and Mufti method, and finite element analysis. The methods are described in detail in Section 2.3.

5.1 Calculation of E and G by CSA standard

As described in Section 2.3.1, the modulus of elasticity (E) and shear modulus of rigidity (G) of masonry wall may be calculated by the following equations:

$$E = 850f'_m \quad (1)$$

$$G = 0.4E \quad (2)$$

The compressive strength of masonry prism (f'_m) are presented in Table 3. Considering those values of f'_m, the calculated values of modulus of elasticity (E) and shear modulus of rigidity (G) of masonry walls can be seen in Table 6.

Table 6: Calculation of *E* and *G* values by CSA standard

Specimen designation	Compressive strength of masonry prism, f'_m (MPa)	Modulus of elasticity, *E* (MPa) $E = 850f'_m$	Shear modulus of rigidity, *G* (MPa) $G = 0.4E$
Wall-1	6.73	5,720	2,288
Wall-2	7.96	6,766	2,706
Wall-3	7.87	6,689	2,676
Average	7.52	6,392	2,557

5.2 Calculation of *E* and *G* by Jaeger and Mufti method

As described in Section 2.3.2, the shear modulus of rigidity (*G*) and modulus of elasticity (*E*) of masonry wall may be calculated by the following equations:

$$G = \left(\frac{h}{ab}\right)\left(\frac{dP}{d\delta}\right)\left\{1 + \frac{4}{r}\left(\frac{h}{a}\right)^2\right\} \quad (3)$$

$$E = r \times G \quad (4)$$

Where *a* is width of wall, *b* is thickness of wall, *h* is height of wall, $(\frac{\mathrm{dp}}{\mathrm{d}\delta})$ is the slope of the active part of the load-deflection curve up to cracking, and *r* is an arbitrary parameter. The following sections demonstrate the calculation of *E* and *G* of masonry walls.

5.2.1 Wall-1

As can be seen in Figure 52 the active part of load-deflection curve up to cracking can be approximated to the green dotted straight line. Slope of the active part of load-deflection curve up to cracking ($\frac{dp}{d\delta}$) is 25 kN/mm.

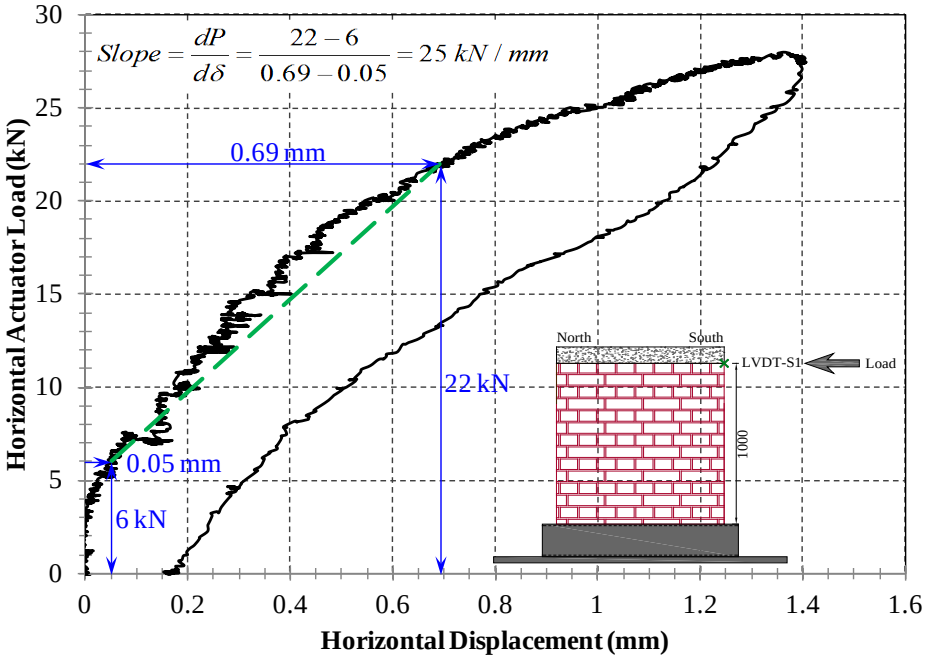

Figure 52: Slope of active part of load- displacement curve up to cracking of Wall-1

Substitution of the actual dimensions of Wall-1 (a = 1040 mm, b = 218 mm and h = 1000 mm) in Equation 3 yields the following equation:

$$G = 110.27 \left(1 + \frac{3.69}{r}\right) N/mm^2$$

Different values of *G* are found by solving the above equation for four different values of *r* as can be seen in Table 7. Substitution of the values of *G* into Equation 4 yields the corresponding values of *E*.

Table 7: *E* and *G* values of Wall-1

r	***G* (MPa)**	***E* (MPa)**
2.5	273	683
3.0	246	738
3.5	227	793
4.0	212	848
4.5	201	903
5.0	192	958
5.5	184	1013
6.0	178	1,069

5.2.2 Wall-2

As can be seen in Figure 53 the active part of load-deflection curve up to cracking can be approximated to the green dotted straight line. Slope of the active part of load-deflection curve up to cracking ($\frac{dp}{d\delta}$) is 7.29 kN/mm.

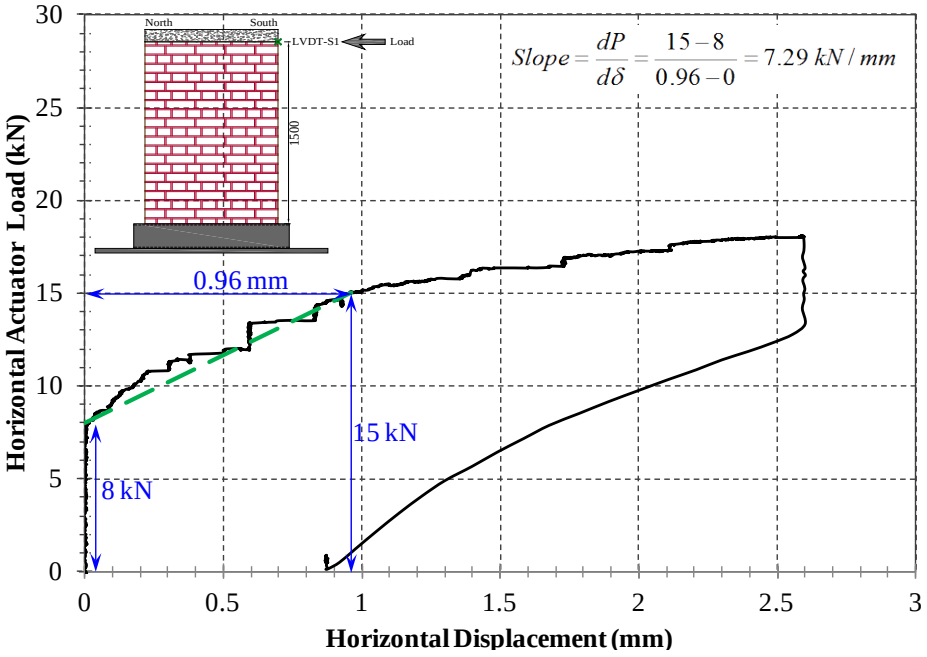

Figure 53: Slope of active part of load- displacement curve up to cracking of Wall-2

Substitution of the actual dimensions of Wall-2 (a = 1018 mm, b = 212 mm and h = 1500 mm) in Equation 3 yields the following equation:

$$G = 50.67\left(1 + \frac{8.69}{r}\right) N/mm^2$$

Different values of G are found by solving the above equation for four different values of r as can be seen in Table 8. Substitution of the values of G into Equation 4 yields the corresponding values of E.

Table 8: *E* and *G* values of Wall-2

r	***G* (MPa)**	***E* (MPa)**
2.5	227	567
3.0	197	592
3.5	176	618
4.0	161	643
4.5	149	668
5.0	139	694
5.5	131	719
6.0	124	744

5.2.3 Wall-3

As seen in Figure 50 LVDT-S1 was not functioning properly. For this reason the load-deflection curve at location of LVDT-N1 rather than LVDT-S1 was used for analysis of Wall-3. As can be seen in Figure 54 the active part of load-deflection curve up to cracking can be approximated to the green dotted straight line. Slope of the active part of load-deflection curve up to cracking ($\frac{dp}{d\delta}$) is 9.14 kN/mm.

Substitution of the actual dimensions of Wall-3 (a = 1015 mm, b = 220 mm and h = 2000 mm) in Equation 3 yields the following equation:

$$G = 81.86 \left(1 + \frac{15.53}{r}\right) N/mm^2$$

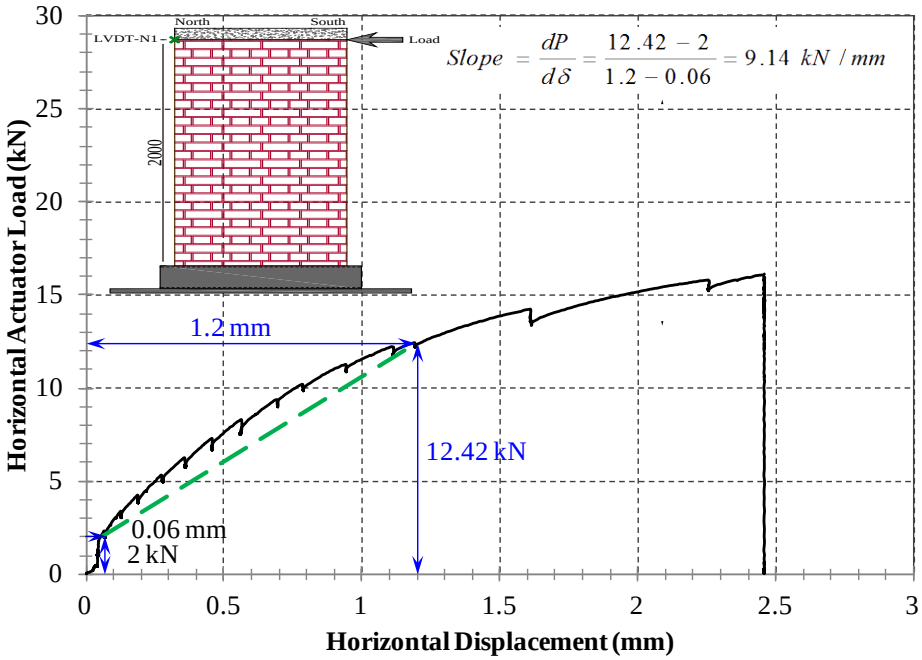

Figure 54: Slope of active part of load- displacement curve up to cracking of Wall-3

Different values of *G* are found by solving the above equation for four different values of *r* as can be seen in Table 9. Substitution of the values of *G* into Equation 4 yields the corresponding values of *E*.

Table 9: *E* and *G* values of Wall-3

r	*G* (MPa)	*E* (MPa)
2.5	590	1,476
3.0	506	1,517
3.5	445	1,558
4.0	400	1,599
4.5	364	1640
5.0	336	1,681
5.5	313	1722
6.0	294	1,762

5.3 Calculation of *E* and *G* by finite element analysis

Finite element analysis (FEA) of masonry walls was conducted to verify the horizontal load versus horizontal displacement behaviour of masonry walls. A computer program developed by Dr. Aftab A. Mufti using FORTRAN computer language was used to conduct the numerical analysis. . The detailed procedure of the finite element analysis is described in Section 2.3.3. The *E* and *G* values of masonry walls by the CSA standard (described in Section 2.3.1 and Section 5.1), and the Jaeger and Mufti method (described in Section 2.3.2 and Section 5.2) were used as input in the finite element analysis

The mesh of finite element analysis models of Wall-1, Wall-2, and Wall-3 are can be seen in Figure 55, Figure 56, and Figure 57 respectively.

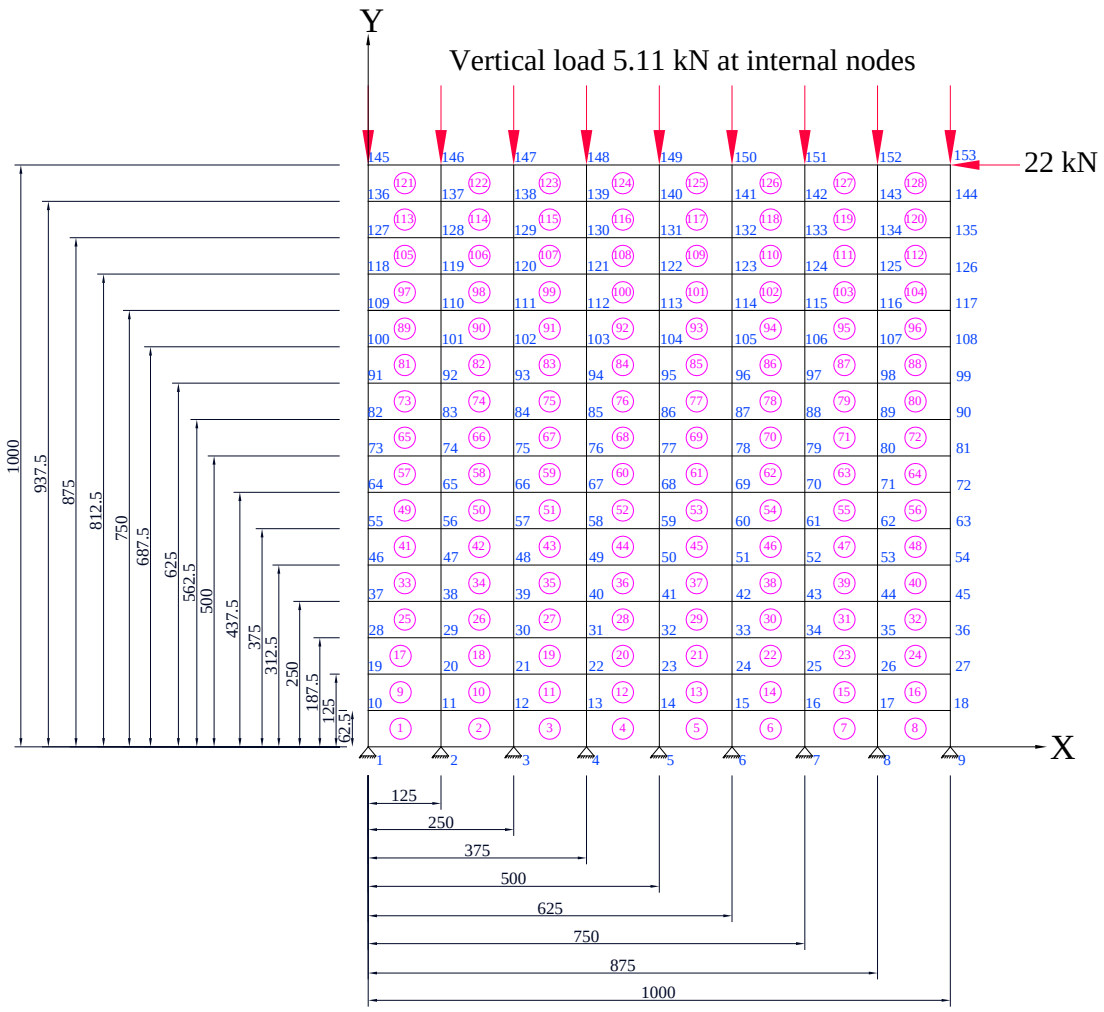

Figure 55: Mesh of finite element analysis model of Wall-1

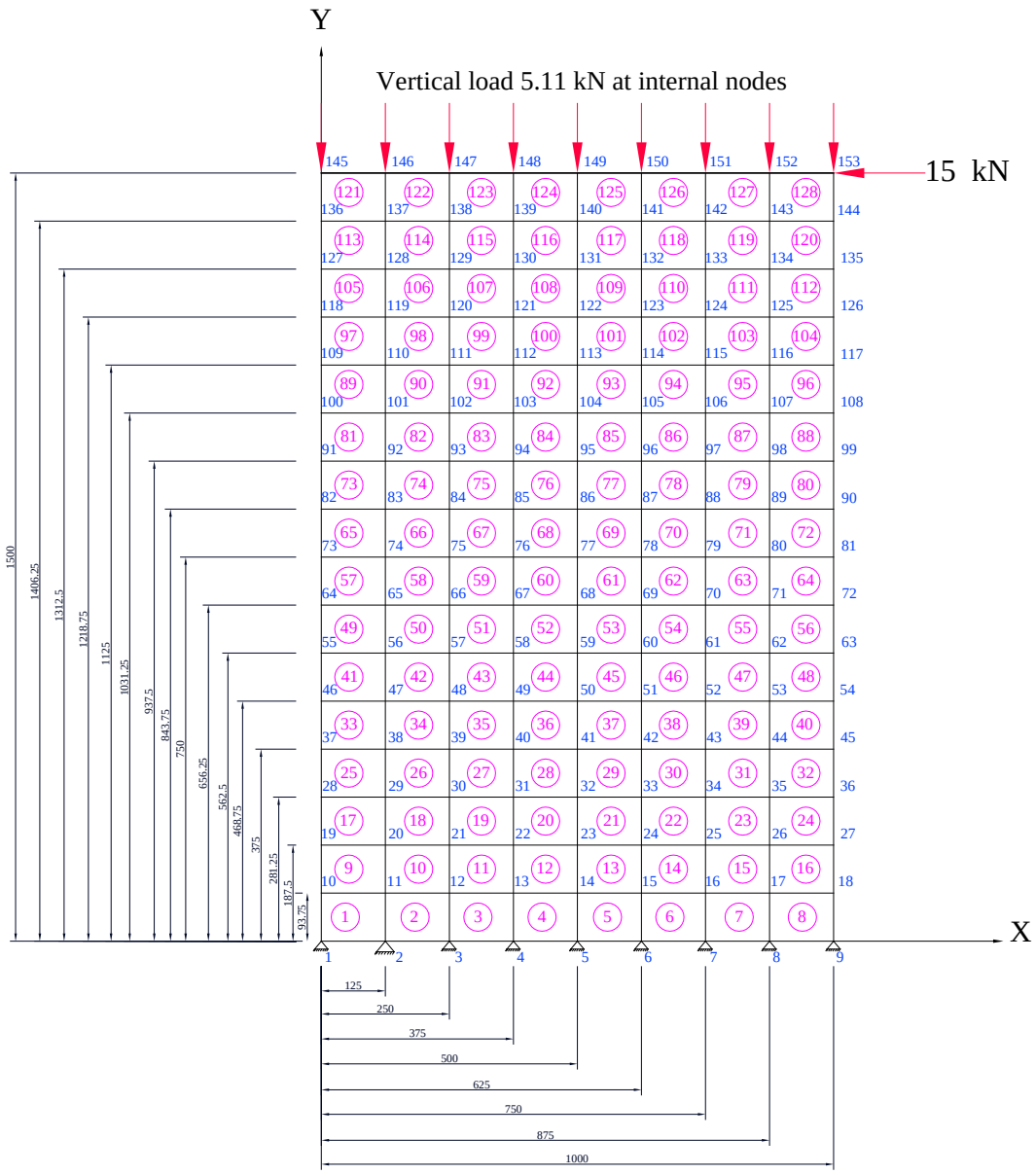

Figure 56: Mesh of finite element analysis model of Wall-2

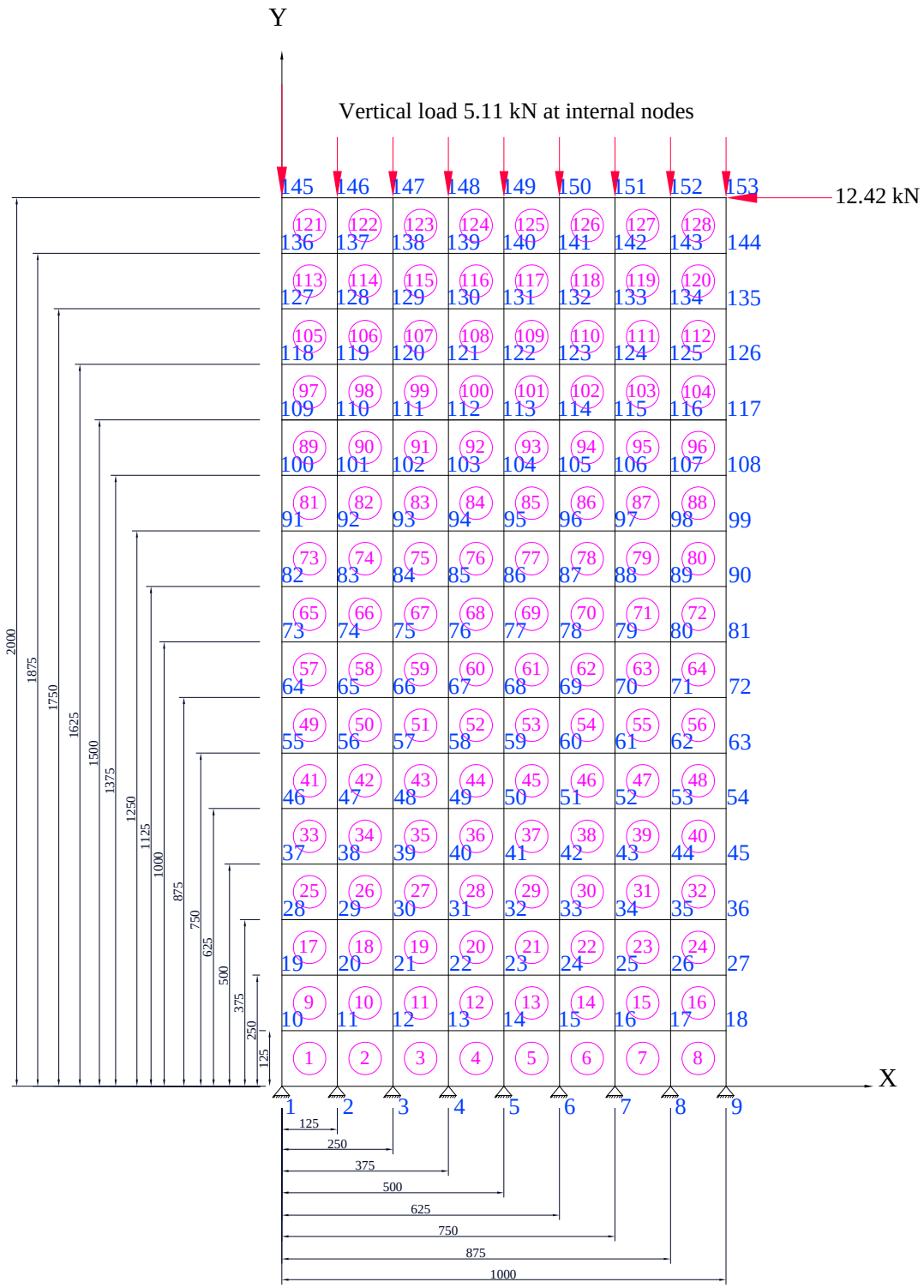

Figure 57: Mesh of finite element analysis model of Wall-3

Figure 58 shows the stress-strain curve of masonry elements, plotted using experimental result, which is described in Appendix A. The initial modulus of elasticity (*E*) is determined from the slope of the linear portion of the curve which is used to calculate the stiffness of all masonry elements.

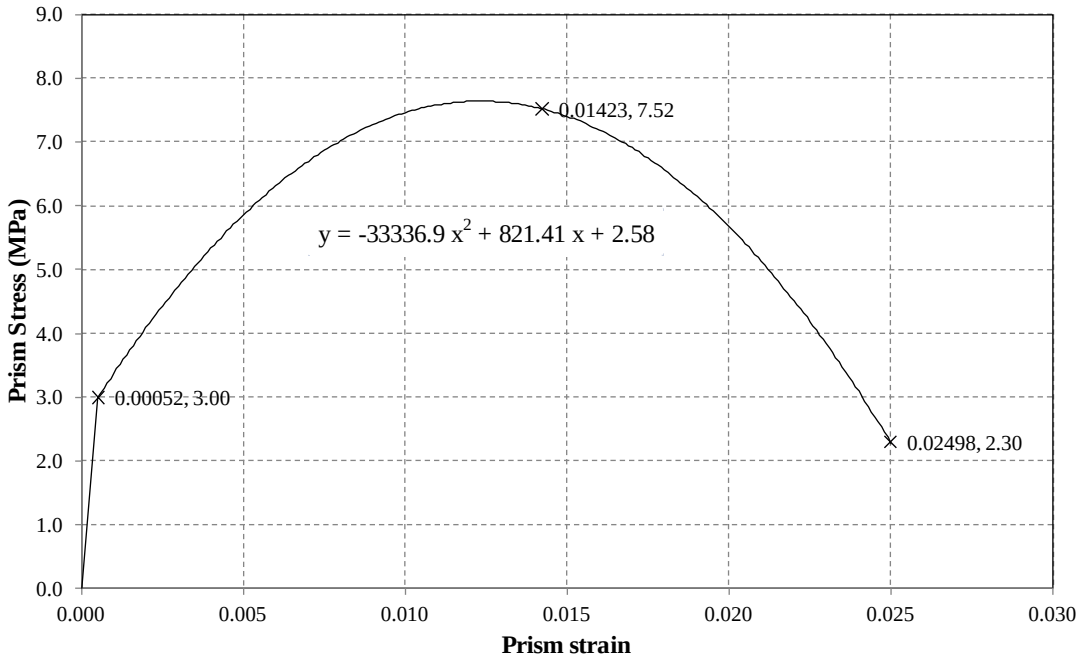

Figure 58: Stress-strain curve of masonry prism in compression

The following sections demonstrate the results obtained from finite element analysis of three masonry walls.

5.3.1 Wall-1

The uncracked load-displacement behaviour of Wall-1 observed from experimental result is compared with that of the finite element analysis results obtained by following the

Jaeger and Mufti method for different values of *r* (2.5, 3, 3.5, 4, 4.5, 5, 5.5 and 6). The comparison can be seen in Figure 59.

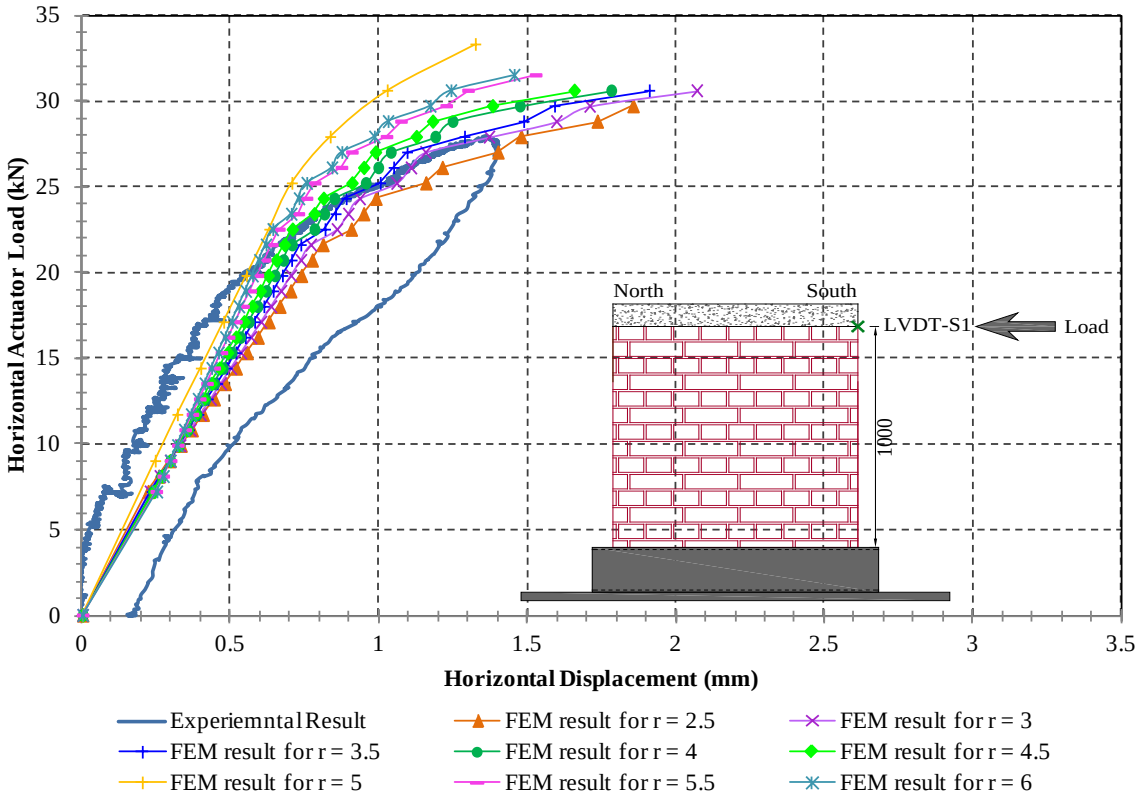

Figure 59: Comparison of experimental result with finite element analysis results of Wall-1

From Figure 59, it is observed that the slope of graphs obtained from finite element analysis for $r = 3$, $r = 3.5$ and $r = 4$ change at approximately 22 kN of horizontal load. During experiment, the first horizontal crack was also visible at 22 kN of horizontal load. Therefore, the horizontal load to initiate first crack obtained from finite element analysis is similar to that of experimental result.

From observation, the finite element analysis results for $r = 3$ match best with the experimental results. Therefore, $r = 3$ is considered to give reasonable estimate of the uncracked effective modulus of elasticity and shear modulus of Wall-1.

5.3.2 Wall-2

The uncracked load-displacement behaviour of Wall-2 observed from experimental result is compared with that of the finite element analysis results obtained by following the Jaeger and Mufti method for different values of r (2.5, 3, 3.5, 4, 4.5, 5, 5.5 and 6). The comparison can be seen in Figure 60.

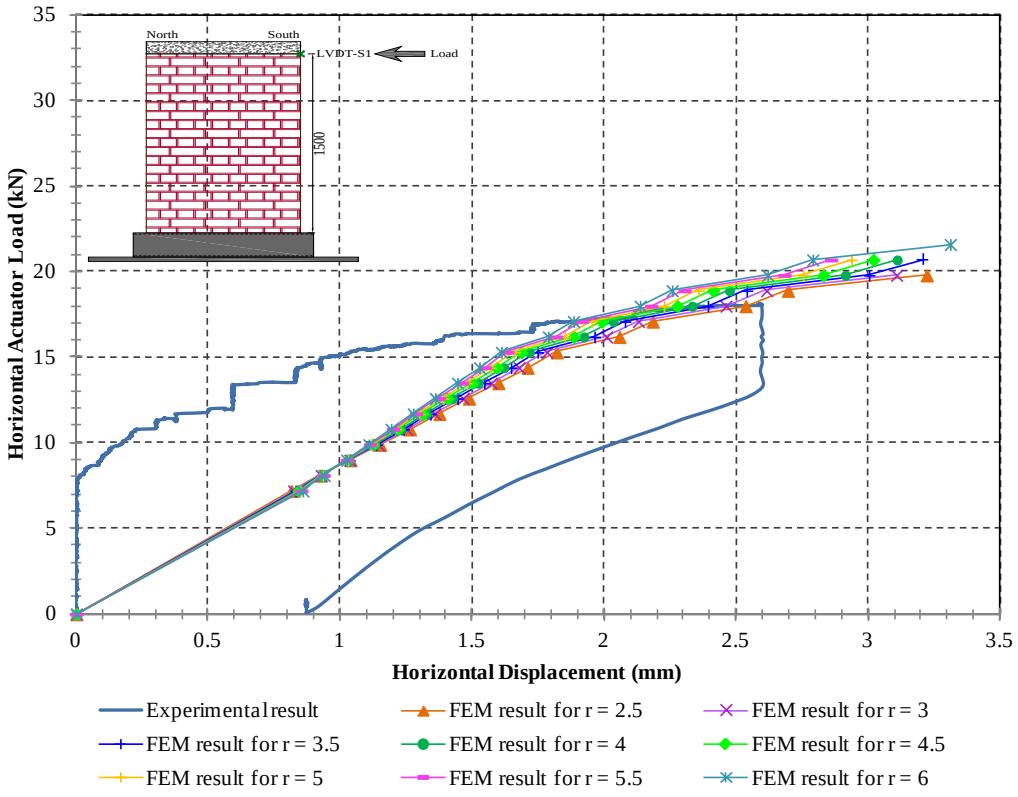

Figure 60: Comparison of experimental result with finite element analysis results of Wall-2

From Figure 60, it is observed that the slope of graphs obtained from finite element analysis for all r values (r = 2.5 to r = 6), change at approximately 15 kN of horizontal load. During experiment, the first horizontal crack was also visible at 15 kN of horizontal load. Therefore, the horizontal load to initiate first crack obtained from finite element analysis is similar to that of experimental result.

From observation, the finite element analysis results for r = 3 match best with the experimental results. Therefore, r = 3 is considered to give reasonable estimate of the uncracked effective modulus of elasticity and shear modulus of Wall-2.

5.3.3 Wall-3

The uncracked load-displacement behaviour of Wall-3 observed from experimental result is compared with that of the finite element analysis results obtained by following the Jaeger and Mufti method for different values of r (2.5, 3, 3.5, 4, 4.5, 5, 5.5 and 6). The comparison can be seen in Figure 61.

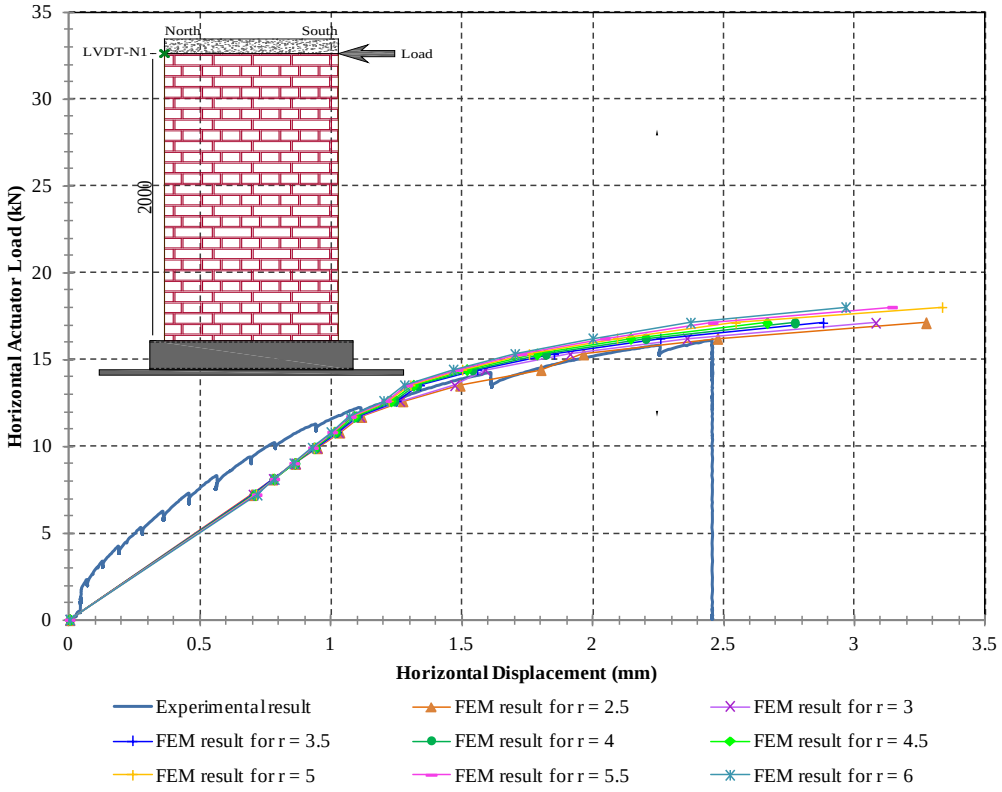

Figure 61: Comparison of experimental result with finite element analysis results of Wall-3

From Figure 61, it is observed that the slope of graphs obtained from finite element analysis for all r values (r = 2.5 to r = 6) change at approximately 12.42 kN of horizontal load. During experiment, the first horizontal crack was also visible at 12.42 kN of horizontal load. Therefore, the horizontal load to initiate first crack obtained from finite element analysis is similar to that of experimental result.

From observation, the finite element analysis results for $r = 3$ match best with the experimental results. Therefore, $r = 3$ is considered to give reasonable estimate of the uncracked effective modulus of elasticity and shear modulus of Wall-3.

5.4 Comparison of experimental results with finite element analysis results

Figure 62, Figure 63 and Figure 64 show the comparison of the following results of masonry walls:

- Experimental results, as described Sections 4.1.1, 4.2.1, and 4.3.1,
- Finite element analysis results using *E* and *G* obtained by the CSA standard, as described in Section 2.3.1 and 5.1.
- Finite element analysis results using *E* and *G* obtained by following the Jaeger and Mufti method for $r = 3$, as described in Section 5.3.

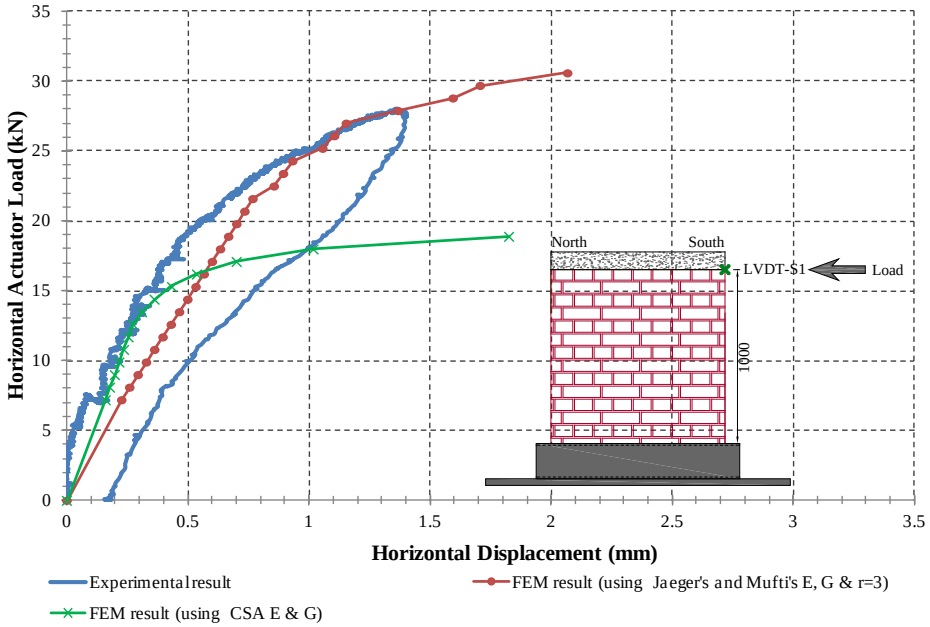

Figure 62: Comparison of experimental results and finite element analysis results of Wall-1

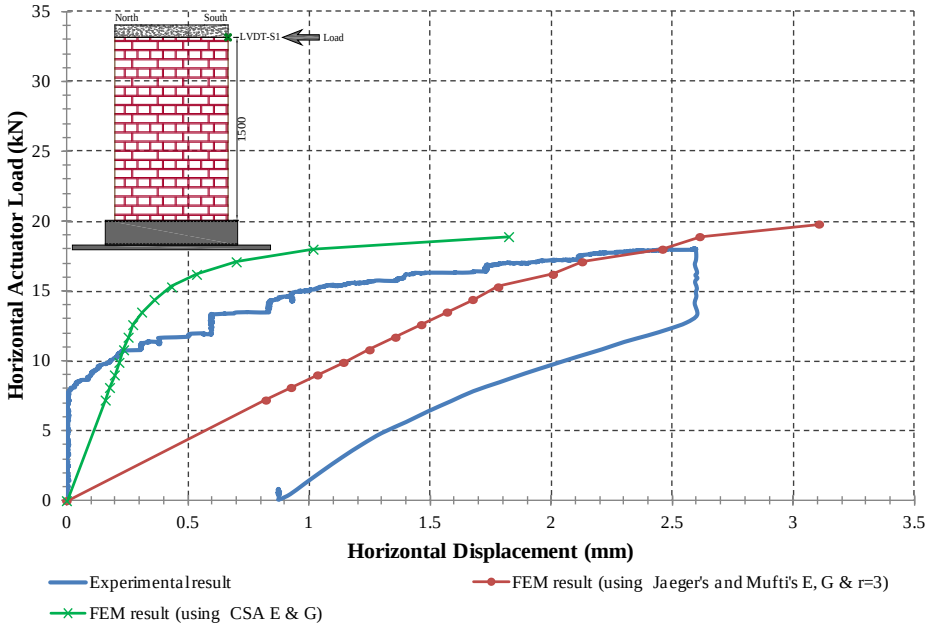

Figure 63: Comparison of experimental results and finite element analysis results of Wall-2

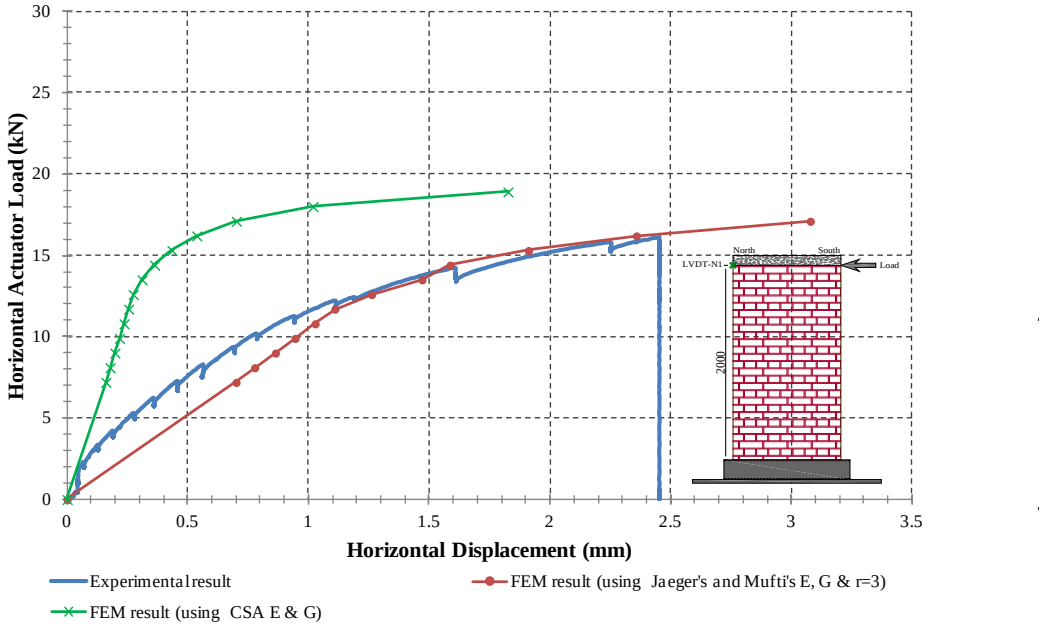

Figure 64: Comparison of experimental results and finite element analysis results of Wall-3

From the comparisons as can be seen in Figure 62, Figure 63, and Figure 64 it is found that load-displacement behaviour of masonry walls obtained from FEA results, using CSA's *E* and *G* values, demonstrate stiffer walls representing higher values of initial lateral stiffness of masonry wall. On the other hand, load-deflection behaviour of walls from FEA results, using the Jaeger and Mufti's proposed *E* and *G* values, demonstrates flexible walls representing lower values of initial lateral stiffness of masonry wall.

It is also observed that the slope of load-displacement curves, determined by FEA results using the Jaeger and Mufti's proposed *E* and *G* values, changes at the similar experimental horizontal load of initiation of first crack.

The Jaeger and Mufti method provides a more conservative solution of designing of masonry walls due to considering lower value of modulus of elasticity.

Chapter 6

Conclusions and Recommendations

The behaviour of unreinforced brick masonry walls under lateral loads were experimentally investigated in this research project. The experimental results were also compared with the finite element analysis results obtained from the theoretical methods proposed by the CSA specifications, and the Jaeger and Mufti method to calculate *E* and *G* of masonry wall. The purpose of the research project was to justify the logic to calculate the effective modulus of elasticity and shear modulus of brick masonry walls by following the Jaeger and Mufti method. Several conclusions and recommendations for future experimental program can be summarized based on the experimental and theoretical results which are presented in the following sections.

6.1 Conclusions

1. The first horizontal flexural cracks were visible at mortar of support-bed joint of walls at tension side.

2. The horizontal load required to initiate first cracking decreased with increment of walls' height.

3. Comparing among the load-displacement profiles obtained from laboratory tests, by the Jaeger and Mufti method, and by CSA specification; it can be concluded that the Jaeger and Mufti method yields conservative values of horizontal deflection at cracking load.

4. From experimental results, it is found that the deflections at initiation of first crack at Wall-1, Wall-2 and Wall-3 are $(\frac{0.69\,mm}{1000\,mm})\ \frac{1}{1450}$, $(\frac{0.96\,mm}{1500\,mm})\ \frac{1}{1563}$ and $(\frac{1.2\,mm}{2000\,mm})\ \frac{1}{1667}$ of the corresponding wall heights. From the above observation it is recommended that for safe estimation the deflection of the wall at initiation of first crack can be considered as $\frac{1}{1200}$ of wall height.

5. The finite element analysis results, using *E* and *G* from the Jaeger and Mufti method for $r = 3$, match best with the experimental results. Therefore, $r = 3$ is considered to give reasonable estimate of the uncracked effective modulus of elasticity and shear modulus of the walls.

6. Both the laboratory tests and finite element analysis of the models validate the Jaeger and Mufti method.

7. *E* and *G* of masonry walls calculated following the Jaeger and Mufti method is effective for design purpose. These values can also be used for rehabilitation of

old deteriorating buildings and strengthening of unreinforced masonry structures subjected to lateral load.

6.2 Recommendations for future research

1. Effects of different magnitude of horizontal and vertical load on the lateral deflection of walls might be investigated.

2. New brick units instead of old units might be used to build the masonry walls that will ensure more homogeneous property of the masonry walls.

3. More investigate on the behaviour of unreinforced brick masonry walls under lateral loads should be conducted to establish the Jaeger and Mufti method to calculate *E* and *G* values.

4. More effective instrumentations should be designed to investigate the in-plane and out-of-the-plane deflection of the walls. One possible option might be to use more sophisticated LMTs (Linear Motion Tandem Transducer) to record the lateral and diagonal deflections of the walls.

References

Akhi, T.P., and Mufti, A.A. (2011). User Manual for FEMS, Non-Linear Analysis of Masonry Structures Using Finite Elements, ISIS Canada Research Network, Winnipeg, Manitoba, Canada.

ASTM (2003). Standard Test Method for Air Content of Freshly Mixed Concrete by the Pressure Method, ASTM C231 / C231M - 03. (2003). *American Society for Testing and Materials,* West Conshohocken, Pennsylvania, USA.

ASTM (2003-a). Standard Test Method for Flexural Bond Strength of Masonry, ASTM E 518-03. (2003). *American Society for Testing and Materials,* West Conshohocken, Pennsylvania, USA.

ASTM (2007). Standard Test Method for Sampling and Testing Brick and Struictural Clay Tile, ASTM C 67-07a. (2007). *American Society for Testing and Materials,* West Conshohocken, Pennsylvania, USA.

ASTM (2007-a). Standard Test Method for Compressive Strength of Hydraulic Cement Mortars (Using 2-in. or [50-mm] Cube Specimens), ASTM C 109/C 109M-07. (2007). *American Society for Testing and Materials,* West Conshohocken, Pennsylvania, USA.

ASTM (2007-b). Standard Test Method for Compressive Strength of Masonry Prism, ASTM C 1314-07. (2007). *American Society for Testing and Materials,* West Conshohocken, Pennsylvania, USA.

ASTM (2009). Standard Test Method for Compressive Strength of Cylindrical Concrete Specimens, ASTM C39/C 39M-09. *American Society for Testing and Materials,* West Conshohocken, Pennsylvania, USA.

CSA (2004). Design of Masonry Structures, CAN/CSA-S304.1-04. *Canadian Standard Association*, Toronto, Ontario, Canada.

Hatzinikolas, M., and Korany, Y. (2005), Masonry Design for Engineers and Architects. *Canadian Masonry Publications*, Edmonton, Alberta, Canada.

Jaeger, L., Mufti, A., Shrive, N., Sorour, M., Duchesn, D, and Paquette, J. (2010), A Suggested Guideline for Seismic Evaluation of Existing Unreinforced Masonry Buildings in Canada, *Proceedings, 3rd International Workshop on Civil Structural Health Monitoring (CSHM-3),* Ottawa, Canada, pp.187-193.

Appendix A

Compressive strength test of masonry prisms

The compressive strength of masonry prisms was determined following the guidelines provided by ASTM C 1314-07 standard specification *(ASTM 2007-b)*. In total five masonary prisms were constructed for each of the walls. The prisms were constructed with five brick units laid in stack bond in stretcher position as can be seen in Figure 65. The height-to-thickness ratio (h_p/t_p) were between 1.3 and 5.0. After construction, the masonry prisms were cured for three days.

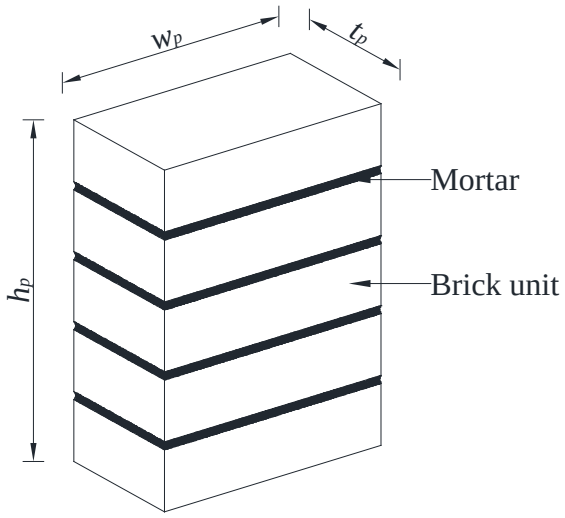

Figure 65: Masonry prism construction

Each of the prisms was capped using a top and a botoom layers of plaster of paris to faciliated the flat surface to tranfer compressive load during test as can be seen in Figure 66. The axial compressive load was applied to the prisms using the MTS machine. The test setup and typical failute pattern of the prisms can be seen in Figure 66. The test result is summarized in Table 10.

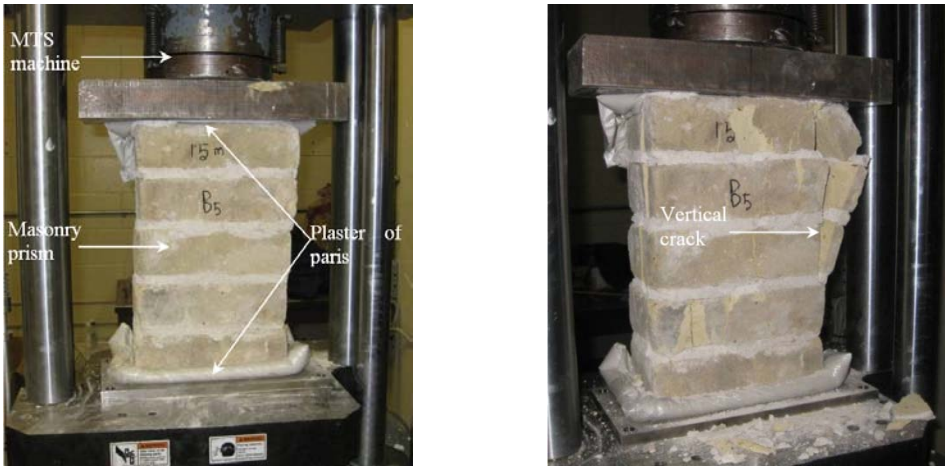

(a) Test setup **(b) After failure**

Figure 66: Typical test setup and failure of Masonry prism under compressive load

Table 10: Masonry prisms' compressive strength test results

Prism representing wall	Specimen designation	Average width of prism (mm)	Average thickness of prism (mm)	Area of prism (mm^2)	Maximum compressive load (kN)	Compressive strength (MPa)	Average compressive strength (MPa)
Wall-1	B1	213	96	20,501	154	7.51	6.73
	B2	210	95	19,903	144	7.22	
	B3	216	99	21,384	134	6.27	
	B4	213	97	20,530	141	6.87	
	B5	218	100	21,825	126	5.77	
Wall-2	B1	217	99	21483	176	8.19	7.96
	B2	215	99	21285	169	7.94	
	B3	212	97	20564	153	7.44	
	B4	216	100	21600	179	8.29	
	B5	212	96	20352	162	7.96	
Wall-3	B1	216	96	20736	165	7.96	7.87
	B2	211	92	19412	153	7.88	
	B3	214	98	20972	156	7.44	
	B4	211	97	20467	163	7.96	
	B5	217	95	20615	167	8.10	

The average maximum compressive strength of masonry prisms of all walls (f'_m) is 7.52 MPa.

The strains and corresponding compressive stresses of the masonry prisms were recorded during the compressive strength tests of masonry prisms. The stress-strain curve plotted using the recorded average compressive stress-strain data can be seen in Figure 67. The parabolic curve for the inelastic portion was drawn considering the curve passes through three known points such as the strain-stress point where the graph changes its slope (0.00052, 3.00 MPa), the average maximum masonry prism compressive strain and corresponding stress (0.01423, 7.52 MPa), and the ultimate masonry prism strain and

corresponding stress (0.02498, 2.30 MPa). The equation of the inelastic portion of the stress-strain curve is as below :

$$y = -33336.9\ x^2 + 821.41\ x + 2.58 \quad (8)$$

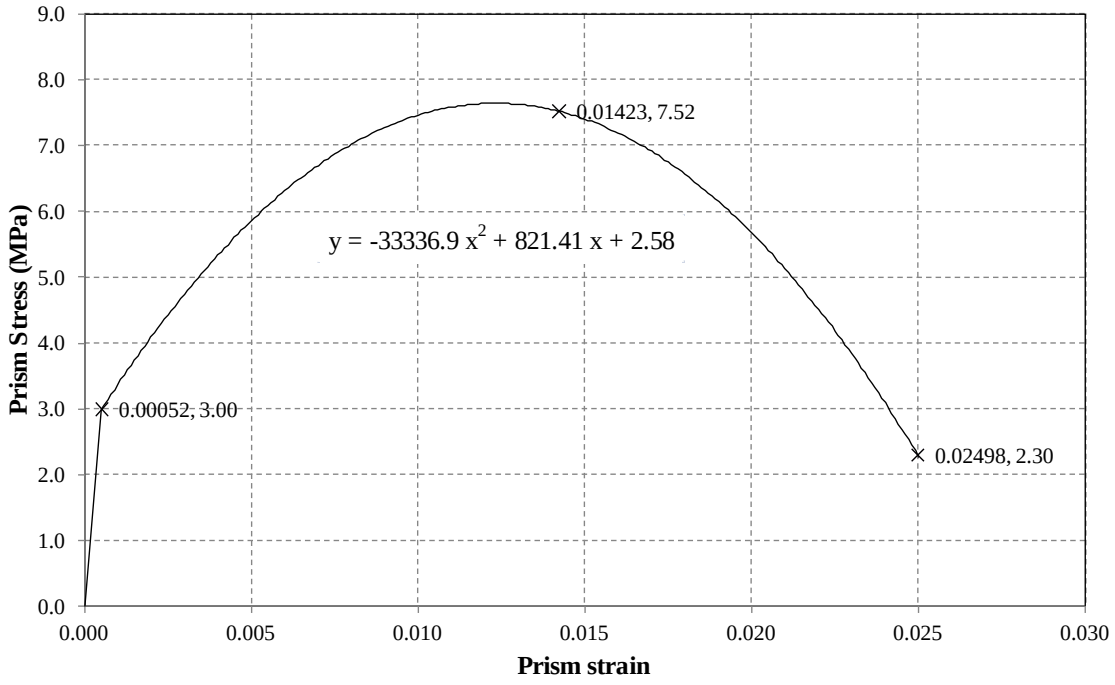

Figure 67: Stress-strain curve of masonry prism in compression

Appendix B

Compressive strength test of brick units

The average compressive strength of the brick units were determined following the guidelines provided by ASTM C 67-07a standard specification (ASTM 2010-a). In total 5 brick units were selected for the test. The brick units were dried in a ventilated oven at 110° C for 24 hours. Then each of the brick units was divided into two pieces using cutting saw, with a length equal to one half of the full length of the unit. Each of the dry half brick specimens were designated as 'A' and 'B' as can be seen in Figure 69. The top and bottom sides of the half brick specimens were capped using sulphur as can be seen in Figure 70. Then the test specimens were tested flat wise (that is, the load was applied in the direction of the depth of the half brick unit). The test results of the compressive strength test are summarized in Table 11. The average calculated compressive strength of the brick units is 34.04 MPa.

Figure 68: Oven dry brick specimens

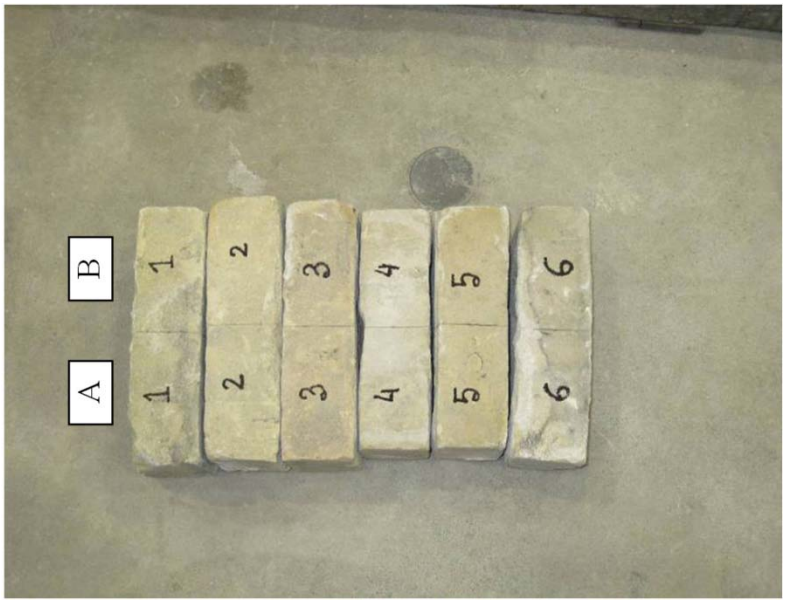

Figure 69: Oven dry half brick specimens

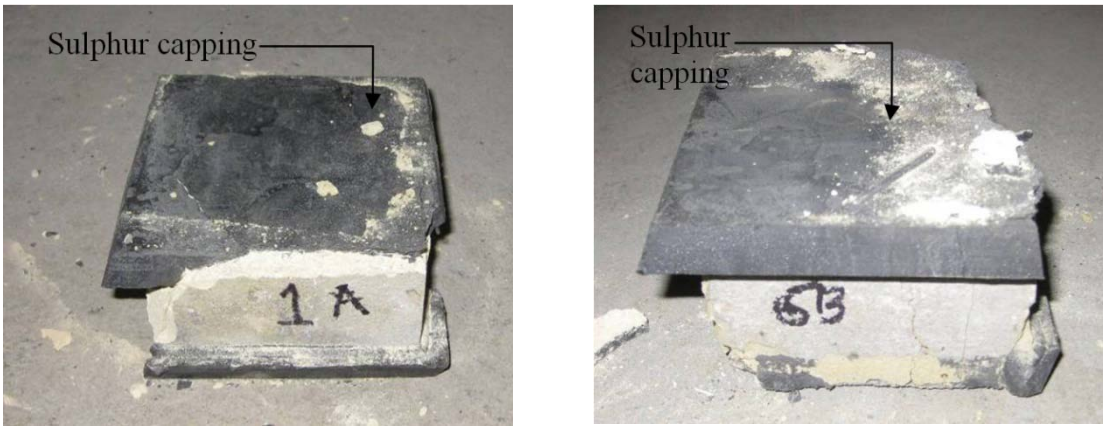

Figure 70: Specimen after compressive strength test

Table 11: Brick units' compressive strength test results

Specimen designation	Face	Average length (mm)	Average width (mm)	Area (mm^2)	Average area (mm^2)	Compressive load (kN)	Compressive stress (MPa)	Average Compressive stress (MPa)
1A	Top	107	101	10795	10747	301	28.00	34.04
	Bottom	106	101	10699				
1B	Top	113	102	11498	11479	364	31.70	
	Bottom	113	102	11459				
2A	Top	109	104	11362	11450	210	18.32	
	Bottom	111	104	11538				
2B	Top	107	98	10486	10445	355	33.99	
	Bottom	103	101	10403				
3A	Top	109	102	11082	11200	212	18.92	
	Bottom	110	103	11318				
3B	Top	110	103	11281	11371	206	18.10	
	Bottom	110	105	11460				
4A	Top	102	96	9752	9767	422	43.20	
	Bottom	101	96	9781				
4B	Top	101	96	9718	9700	413	42.57	
	Bottom	100	96	9681				
5A	Top	102	98	9950	9886	329	33.30	
	Bottom	101	97	9822				
5B	Top	102	98	9955	9993	314	31.43	
	Bottom	103	98	10032				
6A	Top	105	100	10490	10561	613	58.09	
	Bottom	107	100	10631				
6B	Top	106	100	10608	10614	540	50.85	
	Bottom	106	100	10621				